DOI: 10.1070/RCR4594

Nanostructured lead sulfide: synthesis, structure and properties

Stanislav I. Sadovnikov, Aleksandr I. Gusev, Andrey A. Rempel

Institute of Solid State Chemistry, Ural Branch of the Russian Academy of Sciences
ul. Pervomaiskaya 91, 620990 Ekaterinburg, Russian Federation

The theoretical and experimental results of recent studies dealing with nanostructured lead sulfide are summarized and analyzed. The key methods for the synthesis of nanostructured lead sulfide are described. The crystal structure of PbS in nanopowders and nanofilms is discussed. The influence of the size of nanostructure elements on the optical and thermal properties of lead sulfide is considered. The dependence of the band gap of PbS on the nanoparticle (crystallite) size for powders and films is illustrated.
The bibliography includes 222 references.

Contents

I. Introduction 731
II. Methods for the preparation of nanostructured lead sulfide 733
III. The crystal structure of nanoparticles, nanopowders and lead sulfide nanofilms 743
IV. Properties of nanostructured lead sulfide 745
V. Applications of nanostructured lead sulfide 754
VI. Conclusion 755

I. Introduction

Lead sulfide is a representative of the abundant family of semiconducting chalcogenides. It is one of the most demanded narrow-band-gap (0.41 eV for coarse-grained samples) semiconductors. It is used in a number of devices such as photodetectors operating in a broad [from infrared (IR) to ultraviolet (UV)] wavelength range, high efficiency solar cells, thermoelectric transducers and optical switches. Going from coarse-grained to nanostructured PbS has considerably extended the scope of its application, especially in those cases where the particle size is comparable with (or less than) the lead sulfide exciton radius, which is 18 nm.

Energy conversion and storage devices (fuel cells, photoelectrochemical cells for hydrogen production from water, direct solar to electrical energy conversion units, high-capacity cells and energy storage systems) play an important role in the sustainable technology development and in the solution of energetic and environmental problems. The design and the successful use of these devices is dependent on the synthesis of new inexpensive nanomaterials with enhanced performance characteristics. The studies of the last 10 – 15 years demonstrated that nanostructured metal chalcogenides are the most promising materials for the design of high-performance energy conversion and storage devices, detection of radiation over a broad wavelength range, detection of impurities in the gas and aqueous media and for biomedical applications. The synthesis and properties of nanostructured chalcogenides were described in a number of reviews;[1 – 3] however, too broad range of objects inevitably made the discussion too brief.

Sulfur, selenium and tellurium are the three key elements that form chalcogenide compounds. Chalcogenide nanocrystals find wide use in technology. The promising outlook for nanostructured chalcogenides is due to their simple synthesis and unique functional physical and chemical properties (semiconducting or ionic conductivity, mechanical and thermal stability), which can be controlled by changing the size of nanoparticles (grains, crystallites). Moreover, the possibility to control the electrical and optical properties of chalcogenide nanocrystals by changing the size and shape of the nanoparticles obtained in the solvo- or hydrochemical synthesis of colloidal solutions provides for their potential advantages in various applica-

S.I. Sadovnikov. Candidate of Chemical Sciences, Senior Researcher at the Laboratory of Non-stoichiometric Compounds of the ISSC UrB RAS.
Telephone: +7(343)362 – 3034, e-mail: sadovnikov@ihim.uran.ru
Current research interests: synthesis, structure and reactivity of metal chalcogenides, colloid solutions, nanoparticles, nanostructured materials
A.I. Gusev. Doctor of Physical and Mathematical Sciences, Professor, Chief Researcher at the same Laboratory.
Telephone: +7(343)362 – 3523, e-mail: gusev@ihim.uran.ru
Current research interests: non-stoichiometry and ordering in the solid state, thermodynamics, order – disorder phase transitions, nanocrystalline state of condensed matter.
A.A. Rempel. Doctor of Physical and Mathematical Sciences, Professor, Corresponding Member of the RAS, Head of the same Laboratory, Professor at the Division of Physical Methods and Instruments of Quality Control at the Institute of Physics and Technology of the UrFU.
Telephone: +7(343)374 – 7306, e-mail: rempel@ihim.uran.ru
Current research interests: non-stoichiometry, structural defects, order – disorder phase transitions, quantum size effects, nanomaterials, nanotechnologies.

Received 11 August 2015
Translation: Z.P.Svitanko

© 2016 Russian Academy of Sciences and Turpion Ltd.

tions, including photoelectric devices, light-emitting diodes, field effect transistors, biological visualization and many other. The latest achievements in the synthesis of colloidal nanocrystals of lead chalcogenides (PbS and PbSe) and nanocrystals for solar cells can be regarded as a claim for the design of photoelectric and infrared devices based on nanostructured lead chalcogenides. The research of the last decade concerned with the synthesis of nanostructured semiconductor chalcogenides was stimulated, first of all, by the above-listed potential technological applications of these compounds. Nanostructured chalcogenides are synthesized, most often, by 'bottom-up' methods; the most efficient process resulting in the formation of nanocrystals with well controllable size and low size dispersion is the chemical synthesis of chalcogenide colloidal solutions.

Lead, silver, cadmium and zinc sulfides and solid solutions involving them are of most interest among chalcogenides. Out of these nanostructured sulfides, lead sulfide is especially demanded owing to the extensive application.

Before passing to the discussion of the structure and properties of nanostructured lead sulfide and nanomaterials based on it, we will briefly consider the concept of nanomaterials.

Materials, the average particle (grain, crystallite) size of which does not exceed 100 nm, are usually referred to as nanocrystalline or nanostructured.[4–7] In recent decades, it was proved that the decrease in the particle size of a solid below some threshold value can induce a considerable change in the properties, which is called size effect.[5,7–12] The threshold size at which the properties of particles change in a stepwise manner ranges from 1 to 100 nm for most of the materials known to date. The size effects become most pronounced when the particle size is < 10 nm. Since these values are in the nanometre range, the materials exhibiting size effects are called nanomaterials. The particle size of nanomaterials is a highly important characteristic determining the details of properties and the scope of applications.

Formally, any material in which the size of structure elements is of the order of nanometre can be called nanomaterials. However, in this case, the essence of the term 'nanomaterial' narrows down to only defining the size of structure elements; meanwhile, the nanomaterial concept should include not only the size of structure elements but also the stepwise change in the properties resulting from the small size of the elements.[9–11]

The nanostate is intermediate between a molecule and the solid state. The distances at which the main interaction forces in a substance act vary in the range from 1 to 100 nm; therefore, the stepwise change in the properties occurs particularly in the nanometre range.[11] Different types of interactions (electron–electron, electron–phonon, phonon–phonon, magnon–magnon, *etc.*) cover various distances in the same substance. Therefore, the size effects for different properties may appear at different nanoparticle sizes in the same substance.

Nanomaterials are often referred to as nanocrystalline materials. This is not always justified. A material is considered to be nanocrystalline if its structure elements (building blocks, *i.e.*, particles or grains) are crystals. As a rule, nanomaterials are thermodynamically non-equilibrium systems; therefore, their structure elements do not necessarily possess a good crystal structure.[11] Moreover, the building blocks in nanomaterials have a highly defective structure, often approaching an amorphous state. In other words, in the structure elements of most nanomaterials, the long-range order is markedly violated and the many-particle correlations in the arrangement of atoms are provided by the short-range order. Therefore, the term 'nanomaterials' should be understood more specifically as 'nanostructured materials'.

There are various approaches to nanomaterial classification. The most appropriate classification is based on the dimensionality of structure elements that constitute the nanomaterials. The key types of nanostructured materials are zero- (0D), one- (1D), two- (2D) and three-dimensional (3D).[9] By zero-dimensional nanomaterials are meant nanocluster material and nanodispersions, *i.e.*, materials in which the nanoparticles are isolated from one another, and also nanoheterostructures, in particular, quantum dots (QDs). Nanofibrous and nanotubular materials, including quantum wires, are assigned to one-dimensional materials. The length of fibres (rods) or tubes 5–40 nm in diameter can range from 100 nm to tens of micrometres. Nanometre-thick films and semiconductor nanoheterostructures such as quantum wells are classified as two-dimensional nanomaterials. The nanoparticles of 0D, 1D and 2D nanomaterials can occur either in the matrix (liquid or solid) or on a substrate. Three-dimensional nanomaterials are powders and fibrous, multilayer and polycrystalline materials in which 0D, 1D and 2D particles closely adjoin one another and, hence, interfaces are formed between them. A typical example of three-dimensional nanomaterial is a polycrystal with nanometre-size grains. In this nanomaterial, the whole bulk is filled by nanograins, which are virtually devoid of free surface and have only interfaces between the grains.

The physicochemical properties of semiconducting nanomaterials differ substantially from the properties of coarse-grained analogues,[13,14] which is caused by three key reasons:[5,10]

— the nanoparticle size is comparable with the radius of excitons in semiconductors, which affects electronic, optical, luminescent and other properties of nanomaterials;

— small size of grains determines a more extensive surface of the particles; when the grain size is 100 to 1 nm, the surface accommodates 1% to 50% of atoms of the solid, and surface atoms make a considerable contribution to all characteristics of the nanomaterial;

— the proper nanoparticle size approaches the size of a molecule.

Semiconductor nanoheterostructures, especially double ones, including quantum wells, quantum wires and quantum dots, provide the possibility of controlling fundamental characteristics of semiconductors such as the band gap (E_g) and effective masses and mobilities of charge carriers.[10,14–18]

Thus, the 'nanostructured material' concept covers a broad range of objects — from colloidal solutions and isolated nanoparticles to nanoheterostructures of different dimensionality, nanofilms and nanopowders. In line with this, we discuss in this review the preparation methods, structures and properties of lead sulfide colloidal solutions, single nanoparticles, nanofilms and nanopowders. No survey publications devoted to nanostructured lead sulfide are available from Russian or foreign literature. Mention only may be made of a small chapter in a monograph[19] devoted to chemical deposition of PbS films.

The principal methods of synthesis described in the review are general and applicable to the synthesis of any chalcogenide, and the key properties of nanostructured lead sulfide are also typical of other chalcogenides.

II. Methods for the preparation of nanostructured lead sulfide

The most important factors that have to be taken into account in the synthesis of nanoparticles are the following:

— non-equilibrium nature of systems; virtually all nanosystems are thermodynamically unstable; they are prepared under conditions far from equilibrium; this provides active nucleation and, owing to the enormous number of nuclei which accumulate the major part of material, the possible growth of the formed nanoparticles can be appreciably restricted;

— high chemical homogeneity; the nanomaterial homogeneity is achieved if no component separation, either within a single nanoparticle or between the particles, takes place during the synthesis;

— monodispersity; the properties of nanoparticles strongly depend on the particle size; therefore, for the manufacture of materials with good performance characteristics, it is necessary to synthesize particles with rather narrow size distribution.

The preparation processes of nanostructured materials can be classified into two groups according to the way the nanostructure is formed,[11] namely, the bottom-up approach implies the assembly of nanoparticles from atoms and molecules, *i.e.*, the initial species are enlarged to give nanoparticles; the top-down processes are based on disintegration of larger particles or powders to the nanosize.

II.1. Colloidal solutions of lead sulfide nanoparticles

The usual method for the preparation of colloidal solutions of sulfides consists in the chemical reaction between solution components (water-soluble metal salt, sulfidizer and complexing agent) and the termination of the reaction at a definite time point. For certain conditions of synthesis, the dispersion system thus formed can be preserved in the liquid state, *i.e.*, as a colloidal solution. By transferring the liquid colloidal dispersion system to the solid dispersed state, it is possible to precipitate nanosized (or larger) particles from the solution. In the general case, the preparation of a chalcogenide colloidal solution can be conventionally divided into four stages: [20]

— formation of an equilibrium homogeneous complexing agent – water system;

— formation and dissociation of the metal complex $[ML_i]^{n+ik}$ (L is ligand, n is the oxidation state of metal M, i is the number of ligands, k is the ligand charge);

— hydrolysis of the chalcogenizing agent;

— formation of metal chalcogenide.

At the final stage, the dispersed chalcogenide solid phase precipitates or is deposited on the substrate as a film.

A colloidal solution should be considered as stable if during a long period of storage (more than 100 hours), no nanopowder precipitation occurs and the size of nanoparticles present in the solution remains invariable or varies within the error of measurements.

In the vast majority of publications devoted to the synthesis of chalcogenide nanoparticles by chemical bath deposition, the issue of stability of colloidal solutions is not addressed, although only stable colloidal solutions can serve as sources of the smallest-size nanoparticles. An exception is a paper of Deng *et al.*,[21] who consider solubilization, that is, transformation of oil-soluble PbS quantum dots into water-soluble quantum dots, and mention the stability of aqueous colloidal solutions.

Currently, most of colloidal solutions of lead sulfide are synthesized using organometallic compounds.[22–25] Soluble metal complexes are sulfided with hydrogen sulfide gas or hydrosulfuric acid, sodium thiosulfate, sodium sulfide, amide (thioacetamide) or diamide of thiocarbonic acid and their derivatives — thiocarbazide, acetylthiocarbamide and so on. In some cases (usually in the case of solvothermal synthesis), elemental sulfur is used for sulfiding.[26] The particle size is controlled by changing the number of sulfide phase nuclei as they are formed. The use of toxic organometallic lead compounds and organic ligands (thioglycerol, heptane, trioctylphosphine) to prevent agglomeration and growth of PbS particles results in toxicity of the obtained colloidal solutions and restricts the scope of their applicability by ruling out the biological and medical applications.

From the standpoint of a potential biomedical application, hydrochemical synthesis using aqueous solutions of reactants is more acceptable.[27–30] However, in most cases, stability of aqueous colloidal solutions, including lead sulfide solutions, is moderate, ranging from several minutes to 1 – 2 h.

The conditions of synthesis of stable non-toxic aqueous PbS colloidal solutions were elucidated by Sadovnikov *et al.*[30] Lead acetate [$Pb(OAc)_2$] and sodium sulfide served as the sources of Pb^{2+} and S^{2-} ions, while disodium ethylenediaminetetraacetate Na_2H_2 – EDTA (Trilon B) or sodium citrate (Na_3 Cit) functioned as the complexing agents. The initial concentrations of $Pb(OAc)_2$, Na_2S, sodium citrate and Trilon B in the reaction mixtures varied from 0.25 to 25 mmol litre^{-1}. The molar concentration ratio for the reactants in the mixtures was stoichiometric. The colloidal solutions were prepared at room temperature and pH 4.75 – 6.25. According to Sadovnikov and Gusev,[31] the order of addition of the complexing agent to lead acetate or sodium sulfide solutions does not affect the solution stability or nanoparticle size but can give rise to impurity phases. Indeed, in an aqueous solution containing hydrated Pb^{2+}, AcO^- and S^{2-} ions, two dozens of products can appear upon hydrolysis, apart from the colloidal PbS particles.[32] The colloidal solution of lead sulfide nanoparticles is formed upon the following reaction:

$$Pb(OAc)_2 + Na_2S \xrightarrow{Na_3Cit \text{ or } Na_2H_2-EDTA} PbS + 2\,NaOAc \quad (1)$$

In order to estimate the effect of complexing agents on the stability of colloidal solutions, similar solutions were prepared without addition of sodium citrate or Trilon B. In particular, PbS nanoparticles precipitated from reaction mixtures containing equal concentrations of $Pb(OAc)_2$ and Na_2S, either 0.8 or 25 mmol litre^{-1}, within 10 and 60 min after the synthesis, respectively. No stable colloidal solution formed.

The stability of colloidal solutions was evaluated [30] by considering the change in the colloidal nanoparticle size (hydrodynamic diameter D_h) depending on the time (t) of solution storage. The D_h value of PbS nanoparticles directly

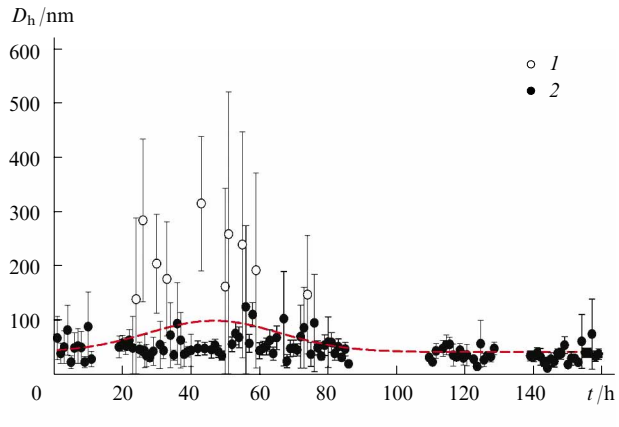


Figure 1. Ranges of D_h values for PbS agglomerates (*1*) and nanoparticles (*2*) in a colloid solution as a function of the solution storage time at room temperature.[30]
The enveloping curve shows the particle size distribution depending on the storage time.

in the colloidal solution was determined by dynamic light scattering.

When Trilon B was added to the reaction mixture, stability of the colloidal solutions increased to 4 days, and by using sodium citrate, it was possible to prepare colloidal solutions that were stable for more than 30 days (they did not change their properties during this period) (Fig. 1). The PbS particle size in colloidal solutions depends on the initial concentrations of lead acetate and sodium sulfide and on the type of the complexing agent. By varying these parameters, it is possible to obtain stable colloidal solutions with a specified particle size ranging from 10 to 20 nm.[30] This process for preparation of colloidal solutions of PbS is protected by a patent.[33]

II.2. Analysis of the formation conditions of lead sulfide in aqueous solutions

It was noted above that, along with colloidal PbS particles, numerous products of hydrolysis are formed in an aqueous solution containing hydrated Pb^{2+}, AcO^- and S^{2-} ions. The important role of metal hydroxide during chemical deposition was discussed in numerous publications (see, for example, Refs 26, 34 and 35). For example, upon chemical deposition from aqueous solutions of thiourea [$(NH_2)_2CS$], metal sulfides are formed as thin films [26, 34, 36, 37] on non-metallic surfaces only in the thermodynamic stability region of metal hydroxide in the solution (hydroxide region). The microstructure of chemically deposited sulfide films depends on the pH value and on the presence of metal hydroxide in the reaction mixture.[38] Metal hydroxide is significant for the assembly of core–shell type sulfide heteronanostructures.[39] Therefore, calculation of the concentration region of formation of metal hydroxide, which allows one to predict the possibility for its appearance in the solution before the sulfide synthesis, is an important task faced by a researcher who performs chemical deposition from aqueous solutions. This calculation is based on comparison of the ionic product with the solubility product of metal hydroxide (K_{sp})

$$K_{sp} = [M^{m+}]\,[HO^-]^m \qquad (2)$$

where $[M^{m+}]$ and $[HO^-]$ are the equilibrium concentrations of free metal ions and hydroxide ions, respectively.

The data on the conditions of formation of lead hydroxide in the $Pb^{2+}-H_2O$ system taking account of the existence of polynuclear hydroxo complexes are scarce. Therefore, a calculation method was proposed [40, 41] and a distribution diagram for complexes in the $Pb^{2+}-H_2O$ system, taking account of all polynuclear hydroxo complexes for which the formation constants are known, was presented.[42]

In aqueous solutions, apart from the insoluble hydroxide, lead ions form soluble hydroxo complexes in which the HO^- ions are the displacing ligands. With HO^- ions, lead forms not only mononuclear $[M(OH)_n]$ but also polynuclear $[M_p(OH)_n]$ neutral or charged hydroxo complexes ($n \geqslant 1$ and $p \geqslant 2$ are integers). In the studies [35, 43–45] devoted to the determination of the formation conditions of hydroxides during the chemical deposition of sulfides and selenides, either only mononuclear hydroxo metal complexes or only some of the polynuclear complexes are taken into account. The elimination of polynuclear hydroxo complexes from consideration results in a noticeable shift of the boundaries of concentration regions.

The equation for the precipitation of $Pb(OH)_2$ in the $Pb^{2+}-Cit^3-HO^--H_2O$ system taking account of soluble lead species [$Pb(OH)^+$, $Pb(OH)_2$, $Pb(OH)_3^-$, $Pb_3(OH)_4^{2+}$, $Pb_4(OH)_4^{4+}$, $Pb_6(OH)_8^{4+}$, $Pb_2(OH)^{3+}$, $PbCit^-$, $Pb(Cit)_2^{4-}$ and $Pb(OH)Cit^{2-}$] has the form [41]

$$C^{Cit}_{Pb,\Sigma} = \frac{K_{sp}[H^+]^2}{K_w^2}\left(1 + \frac{\beta_{11}}{[H^+]} + \frac{\beta_{12}}{[H^+]^2} + \frac{\beta_{13}}{[H^+]^3} + \right. \qquad (3)$$

$$+ \frac{3\beta_{34}K_{sp}^2}{K_w^4} + \frac{4\beta_{44}K_{sp}^3[H^+]^2}{K_w^6} + \frac{6\beta_{68}K_{sp}^5[H^+]^2}{K_w^{10}} +$$

$$\left. + \frac{2\beta_{21}K_{sp}[H^+]}{K_w^2} + \beta_1[Cit^{3-}] + \beta_{12Cit}[Cit^{3-}]^2 + \beta'_1\frac{K_w[Cit^{3-}]}{[H^+]}\right)$$

where K_{sp} is the solubility product of lead hydroxide, K_w is the ionic product of water and β_{ij} are the equilibrium constants for the indicated species.[42, 46]

The dependence of the lead hydroxide solubility on the pH in the presence of sodium citrate, which is shown in Fig. 2, determines the boundary conditions of existence of homogeneous and heterogeneous systems. The homogeneous region, that is, the region of lead existence as only soluble species, *i.e.*, either as a free ion or complex ions, is located below the surface representing the boundary of the $Pb(OH)_2-Pb^{2+}$ heterogeneous equilibrium. Above this surface lies a heterogeneous region in which lead hydroxide is also formed. It can be seen that the solubility of $Pb(OH)_2$ decreases with increase in the pH, and at $[Na_3Cit] = 0$ (*i.e.*, in the $Pb^{2+}-HO^--H_2O$ system), it reaches the minimum value of $\sim 2\times10^{-4}$ mol litre^{-1} at pH $\approx$ 10.5. In the region of pH > 10.5, lead hydroxo complexes are formed; therefore, the total lead concentration in the solution increases.

The increase in the citrate concentration entails an increase in the absolute values of $Pb(OH)_2$ solubility and a shift of the solubility minimum to higher pH.

In the $Pb^{2+}-HO^--H_2O$ system, the position of the precipitation boundary of the $Pb(OH)_2$ solid phase is described by the equation

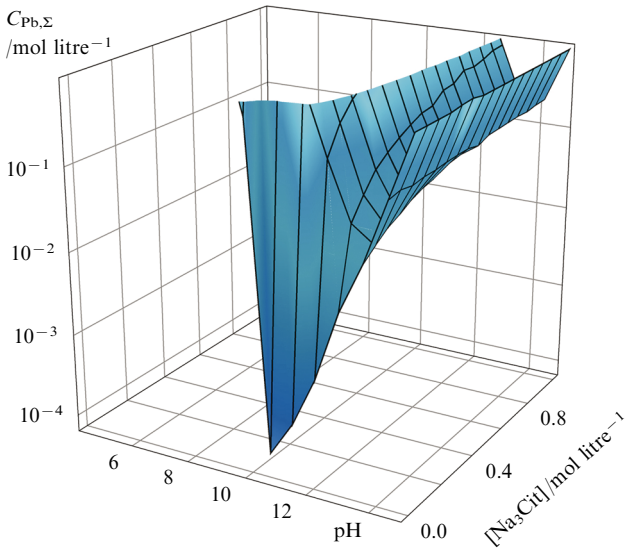


Figure 2. Solubility of $Pb(OH)_2$ as a function of pH of the medium and of citrate ion concentration in the $Pb^{2+}-Cit^{3-}-HO^{-}-H_2O$ system.[41]
The three-dimensional surface is the boundary of the heterogeneous $Pb(OH)_2-Pb^{2+}$ equilibrium. Below this surface, there is the homogeneous region in which lead exists only in the dissolved form, while above the surface lies the heterogeneous region in which $Pb(OH)_2$ is also formed and, upon the introduction of sulfide ions, PbS deposition as a film is possible. The lead concentration $C_{Pb,\Sigma}$ in the solution is presented on the logarithmic scale.

$$C_{Pb,\Sigma} = \quad (4)$$
$$= \frac{K_{sp}[H^+]^2}{K_w^2}\left(1+\frac{\beta_{11}}{[H^+]}+\frac{\beta_{12}}{[H^+]^2}+\frac{\beta_{13}}{[H^+]^3}+\frac{3\beta_{34}K_{sp}^2}{K_w^4}+\right.$$
$$\left.+\frac{4\beta_{44}K_{sp}^3[H^+]^2}{K_w^6}+\frac{6\beta_{68}K_{sp}^5[H^+]^2}{K_w^{10}}+\frac{2\beta_{21}K_{sp}[H^+]}{K_w^2}\right)$$

The positions of the $Pb(OH)_2$ formation boundary in this system determined considering only mononuclear complexes or considering both mono- and polynuclear lead hydroxo complexes are shown in Fig. 3. The effect of polynuclear complexes on the position of the boundary of the $Pb(OH)_2-Pb^{2+}$ heterogeneous equilibrium is especially pronounced in the range of pH < 10.5. In the alkaline region, owing to the amphoteric nature of the lead hydroxide, its precipitation starts and takes place at pH $\leqslant$ 13. When all mono- and polynuclear hydroxo complexes are taken into account, it is possible to obtain PbS films in the alkaline region, 9 < pH < 13 (see Fig. 3 *a*), which is in full agreement with numerous reference and experimental data. If the polynuclear complexes are neglected, the left boundary of formation of lead hydroxide shifts to the acidic region in which no $Pb(OH)_2$ is actually formed. Thus, the inclusion of polynuclear hydroxo complexes into consideration is important not only for theoretical calculations but also for the synthesis of films.

The method of analysis of equilibria taking into account polynuclear hydroxo complexes proposed in the studies cited above[40,41] was also successfully used to determine more correctly the region of formation of lead sulfide in the $Pb^{2+}-Cit^{3-}-HO^{-}-N_2H_4CS-H_2O$ system. The equilibrium established in this system between the PbS precipitate and thiocarbonic acid diamide and lead complexes present in the solution is described by the equation

$$C_{Pb,\Sigma}^{Cit} = \frac{K_{sp,PbS}}{[S^{2-}]}\left(1+\frac{\beta_{11}}{[H^+]}+\frac{\beta_{12}}{[H^+]^2}+\frac{\beta_{13}}{[H^+]^3}+\right. \quad (5)$$
$$+\frac{3\beta_{34}K_{sp,PbS}^2}{[H^+]^4[S^{2-}]^2}+\frac{4\beta_{44}K_{sp,PbS}^3}{[H^+]^4[S^{2-}]^3}+\frac{6\beta_{68}K_{sp,PbS}^5}{[H^+]^8[S^{2-}]^5}+$$
$$\left.+\frac{2\beta_{21}K_{sp,PbS}}{[H^+][S^{2-}]}+\beta_1[Cit^{3-}]+\beta_{12}[Cit^{3-}]^2+\beta'_1\frac{K_w[Cit^{3-}]}{[H^+]}\right)$$

The precipitation boundaries of lead sulfide at different N_2H_4CS concentrations calculated using Eqn (5) are pre-

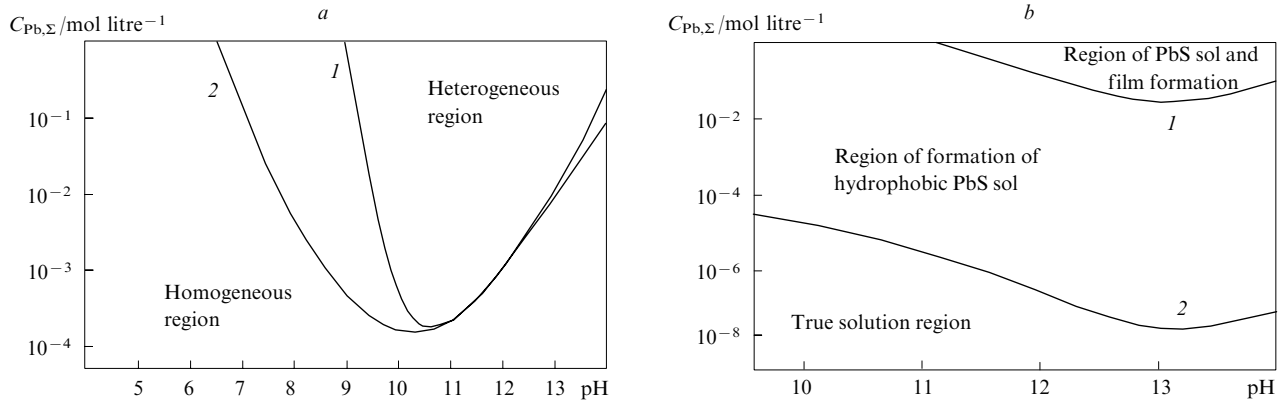


Figure 3. Regions of formation of $Pb(OH)_2$ (*a*) and PbS (*b*).[41]
(*a*) Formation boundaries of $Pb(OH)_2$ in the $Pb^{2+}-HO^{-}-H_2O$ system at 298.15 K: (*1*) considering all mono- and polynuclear hydroxo complexes, (*2*) considering only mononuclear hydroxo complexes; the fields below the boundary curves are the regions of lead existence only in the dissolved form; above the curves lie the heterogeneous regions in which $Pb(OH)_2$ is formed.
(*b*) Regions of formation of PbS as a sol and a film upon deposition from aqueous solutions of N_2H_4CS with a concentration of 0 (*1*) and 0.025 mol litre^{-1} (*2*).

sented in Fig. 3 *b*. Comparison of the formation boundaries of lead hydroxide (see line *1* in Fig. 3 *a*) and PbS indicates that lead hydroxide formed at pH $\geqslant$ 11.1 will be inevitably converted to PbS, because the equilibrium concentration of lead above the $Pb(OH)_2$ precipitate is much higher than above the sulfide.

Generally, the calculation procedure proposed in the cited publications[40,41] is suitable for predicting the formation of solid lead hydroxide and sulfide phases in the solution and choosing the compositions of reaction mixtures required for PbS deposition in various forms: as hydrophobic sol, quantum dots, core–shell heterostructures and films.

II.3. Deposition of lead sulfide nanopowders

The chemical deposition from aqueous solutions is the most popular method used for the synthesis of lead sulfide nanopowders. The size of the obtained nanoparticles depends on the chosen reactants and their concentrations and the temperature of synthesis. Detailed investigations of the conditions of hydrochemical deposition of stable PbS nanoparticles using various reagents are reported in a number of publications.[31,32,47,48]

Stable nanoparticles of the PbS powder were prepared by deposition from aqueous solutions of $Pb(OAc)_2$ (see Refs 31 and 47) or $Pb(NO_3)_2$.[48] An aqueous solution of Na_2S served as the source of sulfur ions. As complexing agents, Na_3Cit or Trilon B were used.

The $Pb(OAc)_2$ and Na_2S concentrations in the reaction mixtures were varied from 1.25 to 100 mmol litre^{-1}, and those of sodium citrate and Trilon B were in the ranges of 0–100 and 0–75 mmol litre^{-1}, respectively. The concentration ratio of lead and sulfur ions was stoichiometric, $[Pb^{2+}]:[S^{2-}] = 1:1$, in all cases.

The solubility product of lead sulfide is low [at 298 K, the K_{sp} value is 2.5×10^{-27} (see Ref. 49) or 8.0×10^{-28} (see Ref. 50)]; therefore, at a relatively high content of Na_2S in the reaction mixture, lead sulfide is formed almost immediately (in 1–2 s). As a result, the reaction mixture first turns black and then, in a few minutes, PbS particles settle down and the solution becomes transparent. The formation of lead sulfide nanoparticles proceeded according to reaction (1), while with lead nitrate the reaction was as follows:

$$Pb(NO_3)_2 + Na_2S \xrightarrow{Na_3Cit \text{ or } Na_2H_2-EDTA} PbS\downarrow + 2\,NaNO_3 \quad (6)$$

All the synthesized PbS nanoparticles with any particle size had a cubic lattice of *B*1 type with the lattice constant $a_{B1} = 0.5902-0.5949$ nm, which is in line with the results of other publications.[51,52] The average particle size of PbS, estimated from X-ray diffraction reflection broadening and by transmission electron microscopy (TEM), varied from 5 to 55 nm, depending on the reactant concentrations.

The contents of lead, sulfur and oxygen in the annealed single-phase PbS nanopowders determined by energy dispersive X-ray (EDX) analysis were 86 ± 2 mass %, 13 ± 1 mass % and 1 ± 0.5 mass %, respectively. According to EDX data, the impurity oxygen present in PbS nanopowders is distributed over the particle surface, the major part being present as adsorbed water and the rest oxygen being in the chemisorbed state.

The concentration of Trilon B influences both the phase composition of the deposited powders and the nanoparticle size. A powder precipitates from a mixture with the minimum Trilon B concentration of 12.5 mmol litre^{-1} contained $\sim$15 mass % of lead sulfate impurity. The lead sulfate and sulfur impurity phases in amounts of $\sim$10 mass % and $\sim$18 mass %, respectively, were found in the precipitates obtained from the reaction mixture with the maximum Trilon B concentration of 75 mmol litre^{-1}. Generally, upon the deposition of PbS powder with Trilon B, the impurity phases are absent only if the $[Pb^{2+}]:[S^{2-}]:$[Trilon B] concentration ratio is from 1 : 1 : 1 to 1 : 1 : (1/2).

As the Trilon B concentration increases from 12.5 to 75 mmol litre^{-1}, nanoparticles measuring 8 to 50 nm are formed (Fig. 4). The increase in the residence time of the synthesized PbS particles in the matrix solution also induces the growth of nanoparticles.

When sodium citrate is used in a reaction mixture with low (1.25 mmol litre^{-1}) concentrations of $Pb(OAc)_2$, Na_2S and Na_3Cit, no lead sulfide precipitate is formed. The deposition of PbS was observed from reaction mixtures containing lead acetate, sodium sulfide and sodium citrate in equal concentrations ranging from 2.5 to 100 mmol litre^{-1}. The precipitates formed from mixtures containing high concentrations of reactants did not contain impurity phases. The particle size varied from 4–5 to 7–8 nm and somewhat increased with increasing concentration of Na_3Cit (see Fig. 4).

Lead sulfide nanopowders consisting of small particles (average size of 5–15 nm) were prepared from reaction mixtures containing $Pb(NO_3)_2$ and Na_2S using sodium citrate as the complexing agent. A change in the Na_3Cit concentration from 12.5 to 50 mmol litre^{-1} does not affect the average PbS particle size to within the error of measurements. When Na_3Cit is replaced by Trilon B, nanopowders with larger particles (up to 20 nm) are formed in reaction mixtures containing $Pb(NO_3)_2$ and Na_2S.

Thus, according to a number of investigations,[31,47,48] the size of lead sulfide particles obtained by deposition from aqueous solutions depends on the reactant concentrations

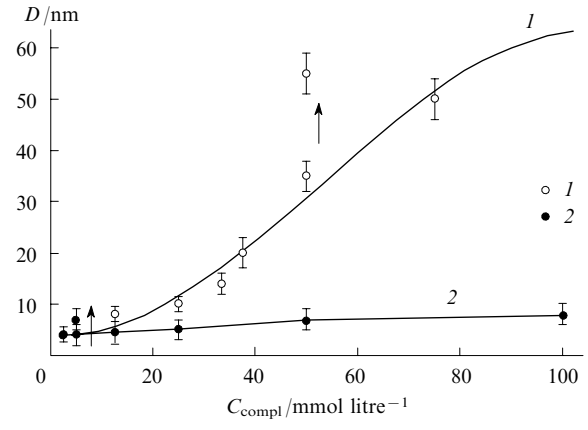


Figure 4. Effect of the concentration of the complexing agents Trilon B (*1*) and sodium citrate (*2*) on the lead sulfide nanoparticle size (*D*) upon deposition from the reaction mixture of lead acetate and sodium sulfide with equal reactant concentrations.[31,47]
The arrows indicate the increase in the PbS particle size after a 70-h (for citrate solution) and 120-h (for Trilon B solution) residence in the matrix solution.

and the type of complexing agent. By varying these parameters, the PbS particle size can be controlled in the range from 5 to 55 nm at 298 K. For the targeted synthesis of PbS nanoparticles of < 10 nm size, it is reasonable to use sodium citrate, while for the preparation of larger particles (up to 50 nm), Trilon B should better be used. Even coarser PbS particles can be obtained by deposition in the temperature range of 330 – 340 K or using thiourea instead of Na_2S.[53]

Uniform cube-shaped PbS nanoparticles with an edge length of 22 nm were obtained by hydrochemical deposition from solutions of lead acetate and sodium thiosulfate in the presence of $C_{17}H_{33}COOK$ as a surfactant.[54]

A sort of bath deposition of nanoparticles is electrochemical deposition. In this case, particles are formed as electrical current is passed.[55, 56] Nanocrystalline PbS is synthesized in an aqueous solution of Na_2S with metallic lead as the sacrificial anode and polyvinyl alcohol as the stabilizer.[57] Upon application of an electrical potential to the electrodes, PbS nanoparticles of 8 – 10 nm size are formed in the solution. According to Yang *et al.*,[55] by varying the potential value and scan rate, it is possible to synthesize PbS nanoparticles with a size in a specified narrow range from 3 to 7 nm. An advantage of electrochemical deposition is the possibility of more accurate control over the nanoparticle size. Also, in the case of long deposition time, it is possible to eliminate unstable compounds from the list of reactants.

Lead sulfide nanoparticles can also be synthesized by a sol – gel process;[58] however, this does not ensure the formation of monodisperse particles.

Lead sulfide nanoparticles and nanostructures are synthesized in spatially confined colloidal systems — colloidal nanoreactors. Most often, these are reverse micelles, liquid crystals, adsorption layers, Langmuir – Blodgett films [59] and microemulsions. The confinement of the reaction zone in which the nanophase is formed provides a high degree of monodispersity for the resulting particles. The molecules that confine the reaction zone should be amphiphilic, *i.e.*, they should have a nonpolar tail soluble in nonpolar solvents, or a hydrophobic tail and a polar hydrophilic head. The amphiphilic properties are inherent in surfactant molecules and ions. When they get in water, surfactant molecules cover the water surface by forming a monomolecular film. In the film, the polar part of the molecule is immersed in water, while the nonpolar hydrophobic substituent is located in air, and the water surface tension is thus decreased. After the surface has been covered, new surfactant molecules and ions pass to the bulk of water.

In non-polar solvents, colloidal structures are formed in which the hydrocarbon tails are arranged at the outward normal to the surface — reverse micelles and water-in-oil microemulsions. In reverse micelles, hydrophilic groups form a polar core, while the hydrophobic tails point outwards. For the chemical synthesis of nanoparticles, reverse micelles are used most often. In order to stabilize the nanoparticles, compounds that modify and coordinate the surface atoms of the particles are added to the micellar solution.[60] As an example, Fig. 5 shows the schematic structure of a PbS nanoparticle with the surface coated by L-cysteine, which serves as the capping agent.[60]

Organometallic synthesis of colloidal chalcogenide nanoparticles in organic solvents in the presence of trioctylphosphine oxide (TOPO) has been reported by Gerion *et al.*[61] A drawback of this method is that the nanoparticles are soluble only in organic solvents. For using these nanoparticles in biological media, it is necessary to endow them with water solubility by forming hydrophilic groups on the surface. The process of particle stabilization and transfer to the aqueous phase is called solubilization. One solubilization method implies the formation of a polymer layer around the nanoparticle.[62] In this case, the hydrophobicity of the TOPO molecules located on the nanoparticle surface is used for binding the hydrophobic groups of solubilizing polymers [block copolymers, polyethylene glycol (PEG) and so on] (Fig. 6). The hydrophilic groups of these polymers point towards the surrounding aqueous solution and form an insulating polar shell. This shell contains active groups for attachment of biological molecules (antibodies, peptides, DNA molecules).

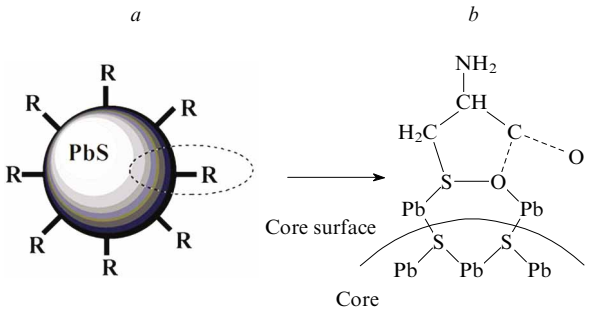


Figure 5. Schematic structure of a PbS nanoparticle with the surface coated by the L-cysteine capping agent (*a*) and a PbS nanoparticle – cysteine coating complex (*b*).[60]
The substituent R is a part of L-cysteine molecule.

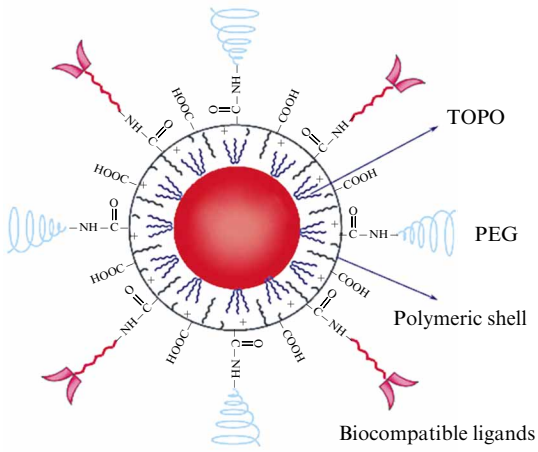


Figure 6. Scheme of the formation of a hydrophilic polymer layer on a quantum dot.[62]
The quantum dot includes a TOPO-coated core and a polymeric shell with an attached amphiphilic PEG layer and biocompatible ligands.

II.4. Deposition of lead sulfide particles with different morphology

The hydro- and solvothermal synthesis at a temperature of > 300 K can be considered as a sort of chemical bath

deposition. Note that in some publications, the chemical bath deposition followed by heat treatment of the resulting lead sulfide powder is erroneously described as hydro- or solvothermal synthesis.

Lead sulfide nanorods ~80 nm in diameter and ~400 nm in length and dendrite nanostructures were obtained by chemical deposition from aqueous solutions of lead acetate and thioacetamide without using ligands or templates.[63] A distinctive feature of this method is the use of solutions of reactants with concentrations differing 5–40-fold. The synthesis was carried out under ambient conditions by adding a highly concentrated solution of one reactant to a solution of the second reactant with a low concentration.

Hydrothermal deposition was used to obtain nanowires and star-shaped PbS crystals,[64] and also well-faceted cubic nanostructures.[65] By using non-aqueous solvents (ethanol, ethylene glycol, ethylenediamine, triethylene glycol, propylene glycol and so on), one can deposit lead sulfide with various particle morphology — dendrite[66–68] and many-arm star-shaped structures,[26,69] separate nanospheres,[70] nanotubes with different cross-section shapes[71–73] and flower-like structures.[74,75] For example, Sun *et al.*[74] prepared flower-like lead sulfide nanoparticles by thermal decomposition of lead diethyldithiocarbamate dissolved in ethylenediamine (the solution was heated by microwave radiation). The reported micrographs[74] indicate that the flower petals are composed of well-faceted cubic or rectangular PbS particles. Shakouri-Arani and Salavati-Niasari[76] prepared 11 different morphological forms of lead sulfide by solvothermal synthesis from $PbNO_3$ and $C_{13}H_{11}NS$. Propylene glycol served as the solvent; the synthesis was carried out at 433 K; and the duration of the synthesis ranged from 8 to 24 h for the preparation of PbS with different morphology.

The micrographs of lead sulfide nanoparticles with different morphology obtained by hydro- and solvothermal synthesis — nanowires and star-shaped crystals,[64] nanotubes,[73] many-arm structures[74] and 'flowers'[75] — are presented in Fig. 7. By ultrasonic treatment of a solution of lead sulfide, it is possible to obtain PbS as separate nanospheres,[69] dendrite structures[67] and nanotubes with a square cross-section.[73]

It was shown[77] that thermal radiolysis (electron beam irradiation) of a solution containing precursors for the synthesis of nanocrystalline PbS gives rise to particles of equal size, *i.e.*, the final material becomes more uniform. As the reactants, the reseachers[77] used solutions of lead acetate and thioacetamide in polyvinyl alcohol.

An interesting method for the preparation of hollow spherical PbS nanoparticles has been proposed.[78] Aqueous solutions of lead nitrate and sodium thiosulfate were used, a thiosulfate solution being slowly added dropwise to a $PbNO_3$ solution. Then the reaction mixture was maintained for 2 h at a temperature of 403 K. First, the lead thiosulfate complex was formed in the solution

$$Pb^{2+} + 2\,S_2O_3^{2-} \longrightarrow [Pb(S_2O_3)_2]^{2-} \qquad (7)$$

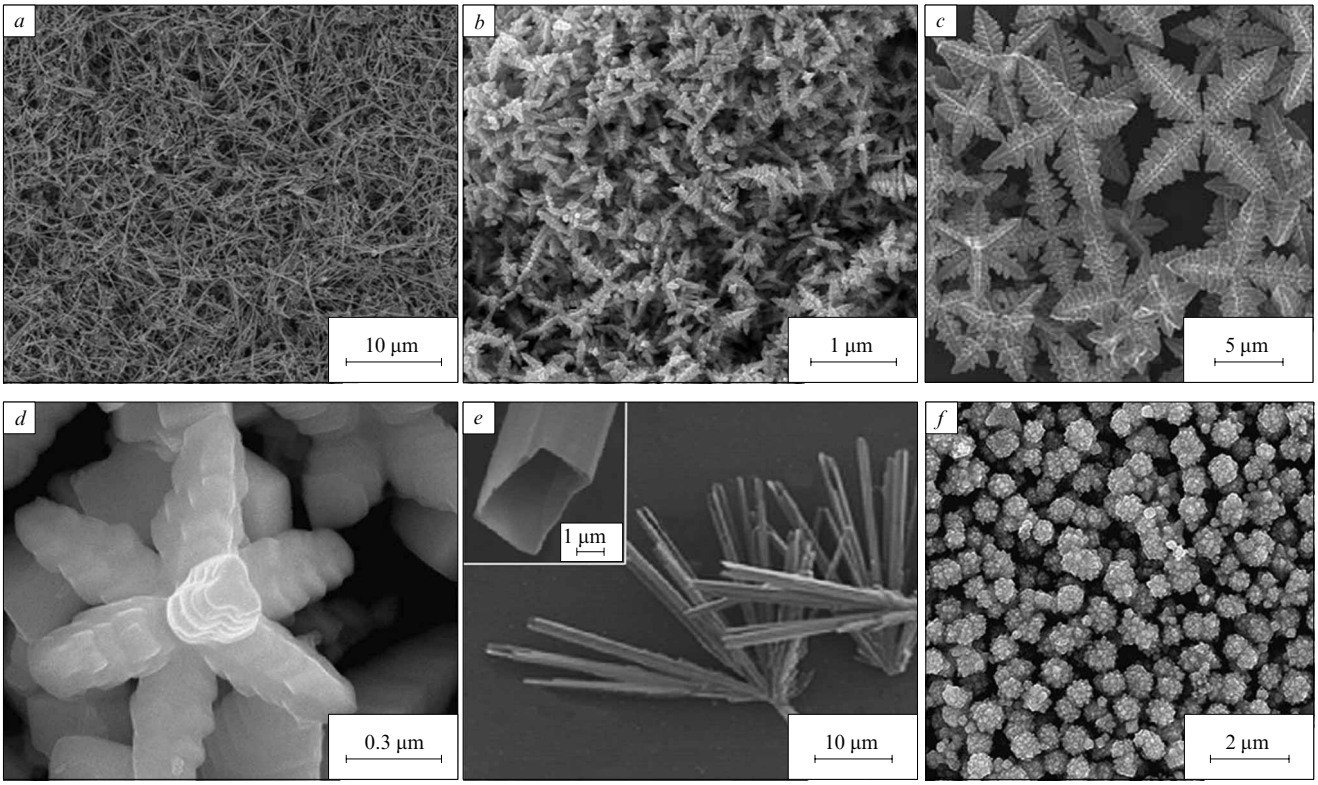


Figure 7. Micrographs of nanoparticles of nanostructured lead sulfide with different morphology obtained by hydro- and solvothermal synthesis.
(*a*) Nanowires,[64] (*b*) dendrites,[68] (*c*) stars,[64] (*d*) many-arm crystals,[74] (*e*) nanotubes with a square cross-section,[73] (*f*) 'flowers'.[75]

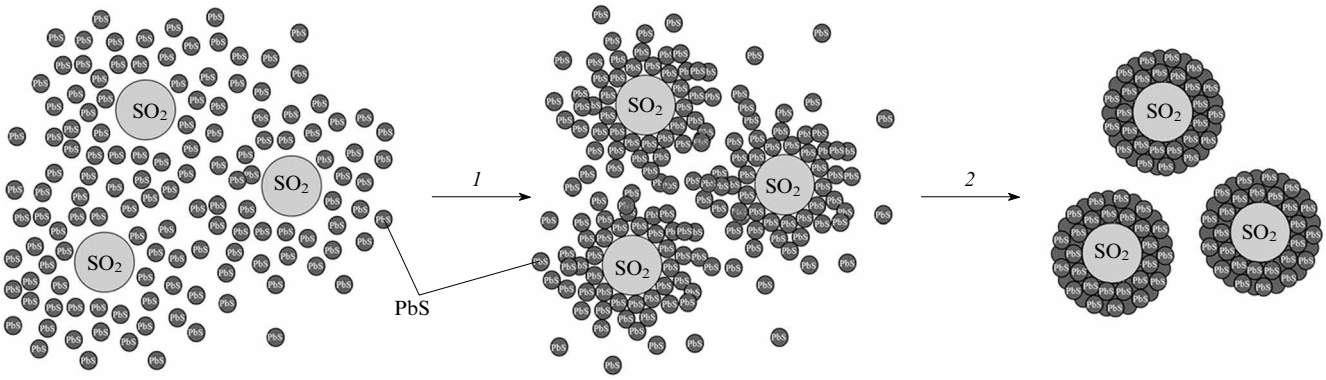


Figure 8. Scheme of formation of hollow spheres from PbS nanoparticles.[78]
(*1*) Aggregation of PbS nanoparticles around SO_2 gas bubbles, (*2*) formation of hollow spheres from PbS nanoparticles.

and on heating, this complex decomposed to give lead sulfide, sulfur and gaseous sulfur dioxide

$$[Pb(S_2O_3)_2]^{2-} \longrightarrow PbS + S + SO_2\uparrow + SO_4^{2-} \quad (8)$$

During the synthesis, PbS nanoparticles of up to 10 nm size were located on the surface of SO_2 gas bubbles and gradually these structures were transformed into hollow spheres 2 – 40 nm in diameter. In other words, SO_2 gas functioned as a template and played the key role in the growth of hollow nanospheres from PbS nanoparticles (Fig. 8).

Thus, hydro- and solvothermal synthesis can produce a variety of morphological types of lead sulfide. The reasons for the formation of PbS particles of different shapes are not entirely clear, as there are very few experimental or theoretical results on this subject in the literature. Probably, the formation of nanoparticles of different morphology is related to their nucleation and growth kinetics. The nanoparticle nucleation and growth are the subjects of only two comprehensive studies [79, 80] carried out for cadmium sulfide nanoparticles by ultrafast small-angle X-ray scattering; data on nucleation and growth of PbS nanoparticle are lacking. The use of elevated temperature for the synthesis promotes the growth of PbS particles; therefore, the characteristic particle size is often beyond the conventional upper boundary (40 – 60 nm [4 – 6, 8 – 11]) of the range defined for nanocrystalline substances.

II.5. Lead sulfide quantum dots

The use of semiconductor quantum dots implies the presence of a matrix. Most often, glass, porous ceramics or substrates are used as QD matrices; therefore, the syntheses of QDs and the matrix are often combined.

Lead sulfide quantum dots are prepared in various media (in glasses,[81 – 84] porous ceramics,[85] films [86] or polymers [87, 88]) and are deposited on various substrates, for example, GaAs.[89]

Okuno *et al.*[81] obtained PbS quantum dots in a low-melting phosphate glass. A mixture of glass powder and PbS was melted at ~1300 K. Then the resulting glass was annealed at ~670 K for a period from several minutes to an hour. After annealing, the glass acquired a brown or black colour as a result of formation of PbS with an average radius of 2 – 3 nm, which is much smaller than the lead sulfide exciton radius (18 nm). The PbS quantum dots with a radius of 1.3 nm were also synthesized by passing hydrogen sulfide through an aqueous solution of polyvinyl alcohol and lead acetate.

del Monte *et al.*[85] grew PbS quantum dots in a hybrid porous organic – inorganic ceramic prepared using 3-mercaptopropyltrimethoxysilane $(MeO)_3Si(CH_2)_3SH$. The growth of the quantum dots is presented schematically in Fig. 9. The quantum dots are formed in the pores of the ceramic saturated with a lead acetate solution in acetic acid with diffusion of gaseous hydrogen sulfide through the ceramic. The growth of lead sulfide QDs is terminated owing to the interaction of the formed PbS particles with a 3-mercaptopropyl group giving a 3-mercaptopropyl shell on the particle surface. Sulfidation was carried out at a temperature of 398 – 418 K for 16 – 32 h. The size of quantum dots obtained under different conditions was in the range from 11 to 14 nm.

An organically modified SiO_2 gel was used [86] as the matrix for PbS quantum dots. A colloidal dispersion of lead sulfide was prepared by a sol – gel process using

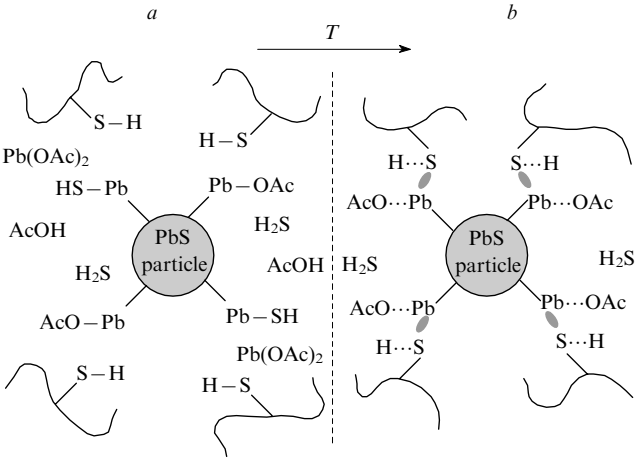


Figure 9. Scheme of PbS nanoparticle growth in the pores of hybrid organic – inorganic ceramics.[85]
(*a*) The formation and growth of PbS particles occur *via* the reaction of lead acetate with hydrogen sulfide; (*b*) interaction of PbS particles with 3-mercaptopropyl to give a 3-mercaptopropyl shell on the PbS particle surface and termination of the particle growth.

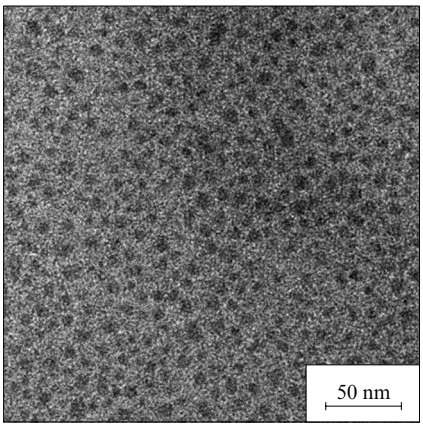


Figure 10. TEM image of PbS quantum dots obtained in an aqueous solution of lead acetate, sodium sulfide and L-cysteine.[60]

complexing agents such as Trilon B and 3-mercaptopropyltrimethoxysilane. Lead sulfide quantum dots with average diameters of 2 and 11 nm, respectively, distributed in a polyvinyl alcohol film, have been studied.[87,88] The chemical deposition of PbS quantum dots from aqueous solutions of lead acetate and sodium sulfide in the presence of L-cysteine as a complexing and stabilizing agent has been considered;[60,90] the size of the resulting lead sulfide QDs was 10 to 20 nm (Fig. 10). The photoluminescence of PbS quantum dots was studied in quite a number of publications.[21,23–25,60,72,81,89,90]

Deng *et al.*[21] proposed a method for solubilization of oleic acid-coated lead sulfide QDs, which provides their transfer into the water-soluble form with high fluorescence. The main idea of the method is that various hydrophilic thiol ligands, including glutathione and L-cysteine, are used as capping agents. Glutathione proved to be especially efficient.

The initial oil-soluble PbS quantum dots were synthesized in two stages. First, lead oleate was prepared from solutions of lead acetate, oleic acid and n-decane at 403 K. Then an aqueous solution of sodium sulfide was added dropwise to this solution; as a result, PbS quantum dots coated by oleic acid were formed and grew at the interface between two liquid phases (water and n-decane). In order to switch to water-soluble QDs, oleic acid molecules were replaced by thiol ligands. The intensity of photoluminescence of the synthesized monodisperse water-soluble PbS quantum dots depended on the sort of the ligand. The highest radiation intensity, which amounted to ~70% of the luminescence intensity of organic QDs, was achieved by using glutathione (Fig. 11 *a*). The radiation intensity of PbS quantum dots with an L-cysteine shell amounted to 20% of the initial intensity. Transition from the initial QDs to water-soluble ones is accompanied by a bathochromic shift of the luminescence maximum from 800 to 890 and 920 nm in the case of glutathione and L-cysteine, respectively (see Fig. 11 *a*). In the opinion of Deng *et al.*,[21] the observed effect is due to the change in the electron density and confinement as a result of formation of Pb–thiol bonds. The formation of these bonds induces also a minor increase in the size of inorganic core of a quantum dot compared with the core of the initial oleic-acid coated PbS quantum dot. Figure 11 *b* shows a TEM image of water-soluble glutathione-coated lead sulfide QDs with an emission maximum at 800 nm. The 4–5 nm quantum dots are uniformly distributed in the solution and, according to electron diffraction data (see the inset in Fig. 11 *b*), they have a cubic structure.

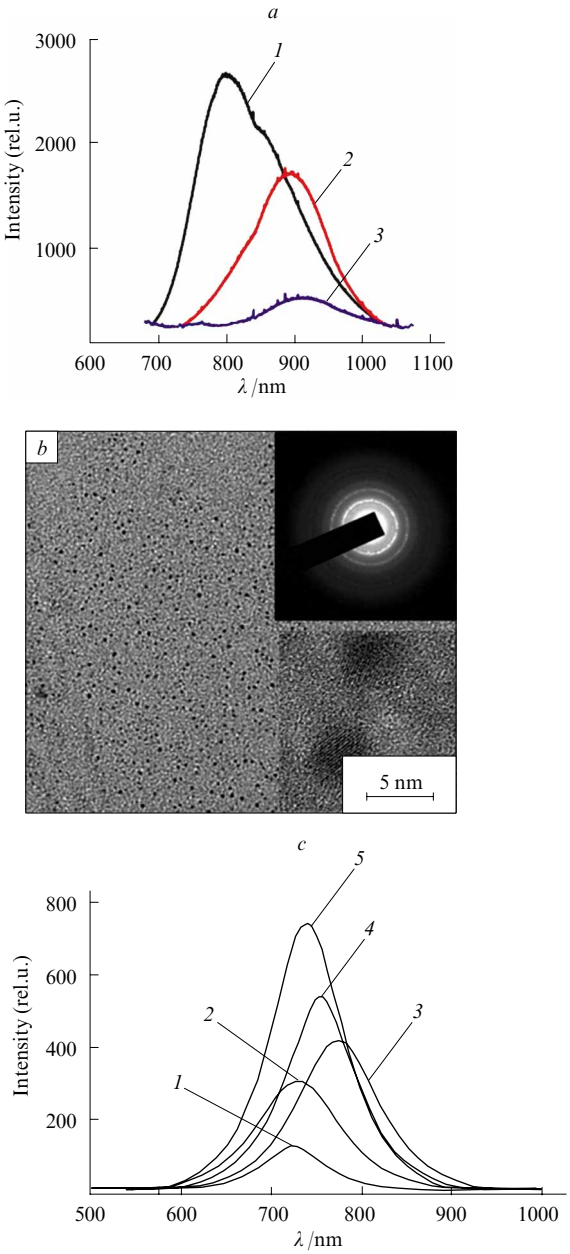


Figure 11. Properties of lead sulfide quantum dots.
(*a*) Influence of the ligand nature on photoluminescence spectra:[31] (*1*) oleic acid-coated QDs; water-soluble QDs: (*2*) glutathione, (*3*) cysteine; (*b*) uniform distribution of monodisperse QDs with a glutathione shell in an aqueous solution (the upper and lower insets show the TEM image and the electron-diffraction pattern of QDs);[18] (*c*) change in intensity and bathochromic shift of the luminescence maximum of the L-cysteine-coated QDs depending on the sulfur to lead concentration ratio in the solution: S : Pb = 0.1 (*1*), 0.2 (*2*), 0.5 (*3*), 0.4 (*4*), 0.3 (*5*).[60]

Yu *et al.*[60] studied the photoluminescence of lead sulfide QDs with a cysteine shell. The 7–8 nm quantum dots were synthesized from aqueous solutions of lead acetate, L-cysteine and sodium sulfide. The highest photoluminescence intensity was found for the QDs synthesized from a solution

with the Pb : cysteine : S concentration ratio of 1 : 2.2 : 0.3; the intensity maximum was observed at a 741 nm wavelength (Fig. 11 *c*). It was demonstrated that photoluminescence of the QDs with a cysteine shell depends on the pH of the medium and S : Pb (see Fig. 11 *c*) and cysteine : Pb concentration ratios in the solution. An increase in the S : Pb ratio induced a bathochromic shift of the emission maximum from 725 to 780 nm. A similar shift of the photoluminescence peak was observed in another study.[21]

Lead sulfide QDs on semiconductor substrates (like GaAs) are grown by the molecular-beam epitaxy method but in this case, a nanoheterostructure is formed.

II.6. Nanostructured lead sulfide films

The methods used to obtain nanostructured chalcogenide films can be classified into chemical and physical ones.

The key chemical methods for the fabrication of nanostructured lead sulfide films include deposition from colloidal solutions, chemical vapour deposition, electrochemical deposition, spray pyrolysis, photocatalytic chemical deposition and successive ionic layer adsorption and reaction (SILAR). Among the physical methods for the preparation of PbS films, the major ones are various alternatives of gas phase deposition (vacuum evaporation, molecular beam epitaxy, glow discharge ion sputtering, ion beam sputtering, ion deposition, reactive ion sputtering, magnetron ion sputtering and high-frequency ion sputtering). Often, combined physical and chemical methods are used to prepare lead sulfide films.[91]

Chemical bath deposition of films is distinguished by simplicity and the possibility to deposit a film on a surface of any size and any configuration; there is no need to heat the substrates to high temperature, and the use of toxic or explosive chemicals is avoided.

Three mechanisms of chemical bath deposition of films can be conventionally distinguished: ionic, cluster (hydroxide or colloid) and ionic cluster mechanisms.[19, 34, 37, 92] In the ionic mechanism, the sulfide nucleation occurs upon the reaction between Pb^{2+} and S^{2-} ions directly on the substrate. According to the cluster (colloid) mechanism, it is assumed that the solid phase nucleation and cluster formation take place in a homogeneous solution, while the growth, coagulation and adsorption occur on the substrate.[19, 43] It is more likely that sulfide films are deposited by a mixed mechanism. In this case, the sulfide is formed both upon the direct reaction between the metal and sulfide ions and upon adsorption of the sulfidizer on the surface of hydroxide particles to form intermediate complexes, which decompose to give the sulfide.

The chemical deposition of PbS films on a glass substrate has been studied in detail.[93 – 98] Three synthetic procedures were used. According to the first procedure, the PbS-1 film was deposited from aqueous solutions of $Pb(OAc)_2$ and $(NH_2)_2CS$ in the presence of Na_3Cit and NaOH without stirring of the solution. In the second procedure, the film was deposited under the same conditions as in the first one but without the addition of sodium citrate, and the deposition was carried out with stirring (PbS-2 film) or without stirring (PbS-3 film). In the third synthetic procedure, the PbS film was formed on the surface of a Trilon-containing aqueous solution of lead acetate owing to the reaction of the latter with hydrogen sulfide gas; the resulting film (PbS-4) was transferred onto a glass substrate. The PbS-1 film was additionally annealed in air at temperatures from 293 to 423 K with a step of 40 K.

The average grain size of a PbS-1 film in the substrate surface was $\sim$250 nm; however, upon a 20 000-fold magnification (Fig. 12 *a*), one can see that the grains are agglomerates of nanoparticles of the $<100-120$ nm size. The degree of continuity of PbS-1 films was not more than 80% – 85%. The PbS-2, PbS-3 and PbS-4 films completely coated the substrate (Fig. 12 *b* – *d*). The smallest nanoparticle size was observed in the PbS-3 film (see Fig. 12 *c*). In the PbS-4 films (see Fig. 12 *d*), all grains were well-faceted and the size of most grains was <120 nm. The smaller particle size of PbS-2 and PbS-3 films compared with PbS-1 is due to the fact that the deposition was carried out without sodium citrate. In the absence of sodium citrate, the rate of formation of PbS nuclei decreases but the number of the nuclei increases, which results in a relative decrease in the particle size. The observed size of PbS nanoparticles in the films varies over a broad range, from 10 to 160 nm, the average size being 50 – 70 nm.[95, 98]

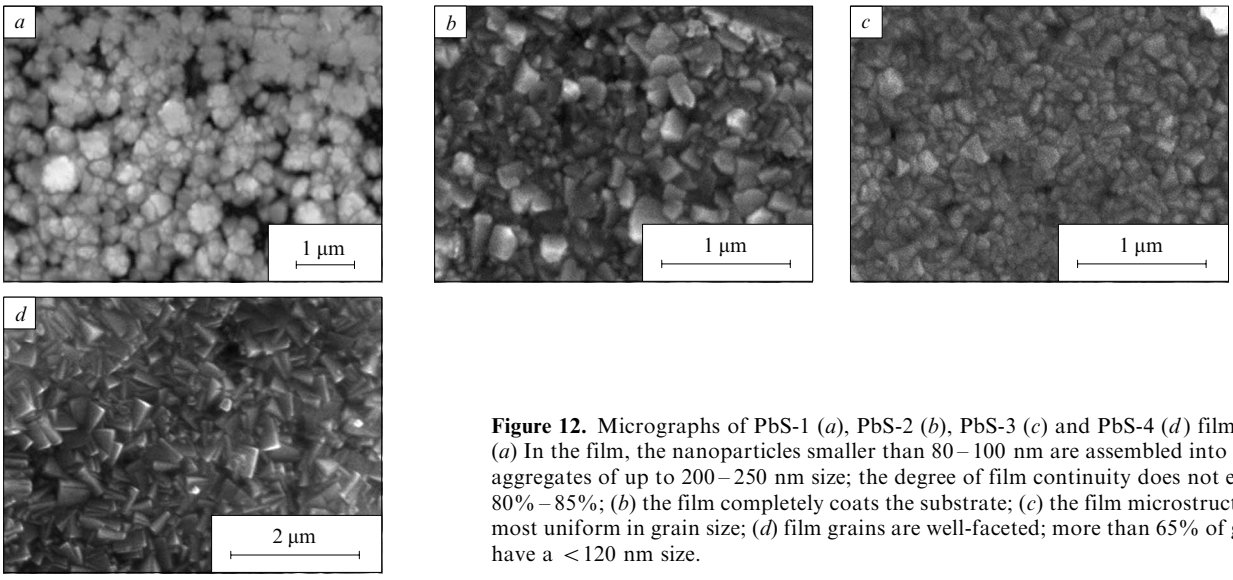


Figure 12. Micrographs of PbS-1 (*a*), PbS-2 (*b*), PbS-3 (*c*) and PbS-4 (*d*) films.[98] (*a*) In the film, the nanoparticles smaller than 80 – 100 nm are assembled into larger aggregates of up to 200 – 250 nm size; the degree of film continuity does not exceed 80% – 85%; (*b*) the film completely coats the substrate; (*c*) the film microstructure is most uniform in grain size; (*d*) film grains are well-faceted; more than 65% of grains have a <120 nm size.

A simple method for the preparation of nanostructured PbS films, ensuring a specified range of band gap energies, has been proposed.[99] Lead sulfide nanofilms active in the near-IR range were prepared by deposition from aqueous solutions of lead acetate and thiourea in the presence of sodium citrate and sodium hydroxide; the solution pH was 10–13. By varying the reactant concentration ratio, PbS films with a controlled average particle size ranging from 35 to 80 nm were obtained.

In the case of chemical vapour deposition,[100] the substrate is exposed to vapour of one or several compounds or to reactive gases which are components of the deposited material. The compound is formed *via* layer-by-layer condensation of atoms (molecules), similarly to the preparation of semiconductors using physical deposition methods (evaporation or ion sputtering). The difference is in the fact that in the case of chemical vapour deposition, the product arises as a result of heterogeneous chemical reaction. The advantages of this method include the possibility of high-rate deposition and doping and growing of epitaxial layers with low impurity contents. However, this method also has disadvantages, including the complexity of deposition and the necessity to heat the substrate to high temperature, which restricts the choice of the substrate material.

The spray pyrolysis method [101, 102] implies spraying a solution, most often, aqueous one, containing salts of components of the deposited compound onto a heated substrate. As the sprayed solution hits the hot substrate surface, it pyrolytically decomposes, and the reaction product forms separate crystallites or groups of crystals on the surface. This method is suitable for the preparation of films with strong adhesion to the substrate and high mechanical strength, stable under ambient conditions and at elevated temperature. A drawback of this method is the absence of direct correlation between the compositions of the deposited compounds and the sprayed solution.

The SILAR method for the preparation of thin films proposed in 1985 [103] and patented in 1987 [104] is based on the heterogeneous reaction taking place at the liquid/solid interface between the Pb^{2+} cations adsorbed on the substrate and the S^{2-} anions located in the solution.[20, 105–109] This method is schematically shown in Fig. 13. The purified substrate is placed into a solution containing Pb^{2+} cations (stage *1*), which are adsorbed on the substrate surface. In stage *2*, the surface is cleaned from non-adsorbed lead cations. A lead sulfide nanolayer is formed in stage *3*, when the substrate bearing the adsorbed Pb^{2+} ions is dipped into a solution containing S^{2-} anions. As a result of reaction between the sulfide anions and lead cations, a thin layer of lead sulfide is formed (stage *4*). The deposition process repeated many times provides a layer-by-layer growth of the PbS film of a specified thickness with particles of a desired size on substrates of different type and shape.[105–109]

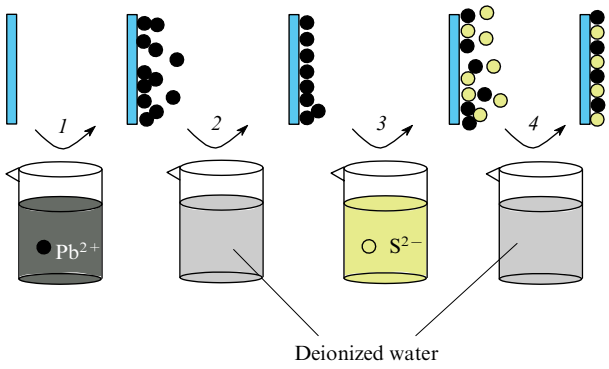


Figure 13. Schematic diagram of the SILAR method.[109] For stages *1–4*, see the text.

The successive layer ionic deposition as a preparation method for thin-film coatings is an upgraded hydrochemical deposition method, which makes it possible to control the morphology and thickness of the obtained films.[105–109] By using various reagents and by varying their concentration and the number of deposition cycles, it is possible to grow polycrystalline PbS films with predominant particle growth along a particular crystallographic direction.[106]

An interesting method is photocatalytic chemical deposition of films.[110, 111] Zhukovskiy *et al.*[111] dipped a TiO_2 nanofilm on a glass substrate into a lead acetate and sulfur solution in ethanol. The TiO_2 nanofilm served as the catalyst. When this system was exposed to light, the following processes took place: photocatalytic reduction of sulfur with ethanol, the formation of lead sulfide and deposition of 4–10 nm PbS nanoparticles on the TiO_2 surface. The problems of manufacture of photocatalysts by depositing PbS on TiO_2 are considered in a review.[112]

Thin nanostructured films are formed by vacuum evaporation followed by deposition and molecular-beam and gas phase epitaxy. Because of specific features of the deposition process (high vapour supersaturation, specific condensation kinetics, sharp change in the velocity of vaporized atoms on going to the absorbed state), the resulting fine-grained nanofilms are thermodynamically non-equilibrium and contain a large number of 'frozen' structural defects. Therefore,

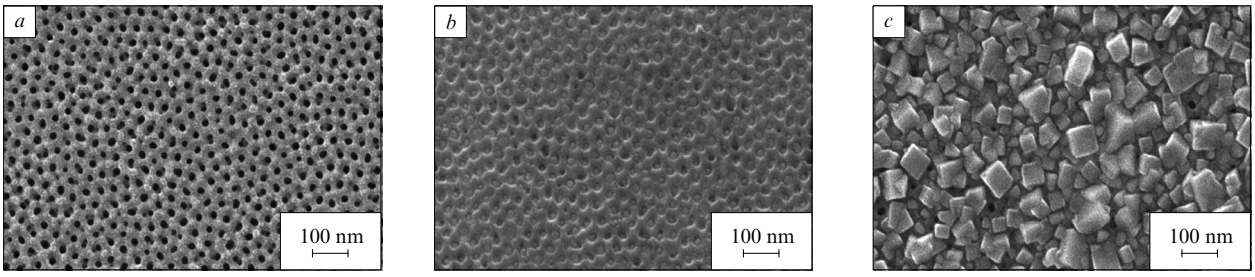


Figure 14. SEM images of Al_2O_3 membrane with pores of 20 nm diameter (*a*), metallic lead nanofibres obtained by injection of a lead melt through membrane pores (*b*) and PbS nanoparticles obtained by sulfidation of lead nanofibres with hydrogen sulfide (*c*).[113]

this method is more suitable for the preparation of lead sulfide nanocrystals without aggregation on a large surface area.

Well-faceted PbS nanoparticles on an Al_2O_3 substrate were obtained [113] by a combined physical and chemical method. A porous membrane with 20 nm holes was used as the template. A metallic lead melt heated to 673 K was hydraulically injected through the membrane nanopores. Sulfidation of lead nanowires was carried out by gaseous hydrogen sulfide. This gave a dense layer of PbS nanoparticles of 100 nm and smaller size (Fig. 14).

Thus, a number of chemical and physical methods for the synthesis of nanostructured lead sulfide as colloidal solutions, nanoparticles, nanopowders and films has now been developed.

III. The crystal structure of nanoparticles, nanopowders and lead sulfide nanofilms

The bulk lead sulfide is commonly regarded as a stoichiometric compound with a negligibly narrow homogeneity ($PbS_{0.9995-1.0005}$).[114] Under a normal atmospheric pressure and room temperature, lead sulfide crystallizes in a cubic (space group $Fm\bar{3}m$) *B*1 structure with the lattice constant $a = 0.59362$ nm. The lead and sulfur ions occupy sites 4(*a*) with coordinates (0 0 0) and sites 4(*b*) with coordinates (1/2 1/2 1/2), respectively.

Under a pressure of 2.5 GPa, lead sulfide with the *B*1 structure acquires orthorhombic *B*16 (*B*33) structure, *i.e.*, a phase transition of cubic *B*1 structure to orthorhombic (space group *Pnma*) structure of the GeS type takes place.[114] As the particle size decreases, the surface energy increases; therefore, the pressure needed to change the crystal structure should increase. Indeed, in a PbS nanopowder, a cubic to orthorhombic phase transition starts at a higher pressure (3.0 GPa).[115] According to the data of Qadri *et al.*,[115] the phase transition is sluggish. The smaller the grain size, the more sluggish the transition. The two phases with the *B*1 and *B*16 (*B*33) structures can coexist up to 8 GPa. As the pressure increases to 25 GPa, a second phase transition of lead sulfide to a CsCl type (*B*2) cubic structure takes place.[116]

Recent studies showed that the decrease in the grain size of sulfides to several tens of nanometres (and below), *i.e.*, the transition to the nanostructured state, is accompanied by a noticeable change in their optical properties.

The transition to the nanostate is accompanied by not only transformation of the properties of sulfides associated with size effects but also by structural changes. In particular, cadmium sulfide as single crystals or coarse-grained powders crystallize in the hexagonal wurtzite (*B*4 type) [117] or cubic sphalerite (*B*3 type) type structures.[118, 119] However, CdS thin films or nano- or ultradisperse powders have a structure different from the crystal structure of these two modifications. Recently, it was shown [120, 121] that CdS nanoparticles have a specific disordered structure with random alternation of close-packed atomic planes; the mean lattice of this disordered structure is described by space group *P*6/*mmm*.

The data on the crystal structure of PbS films are also ambiguous. It is usually assumed that PbS films, like coarse-grained bulk lead sulfide, have a stoichiometric composition and a cubic *B*1 structure (space group $Fm\bar{3}m$). On the basis of investigating the structures of PbS films at different temperatures, Quadri *et al.*[122] suggested that at 375 K, weak phase transition from the *B*1 to cubic *B*3 structure (space group $F\bar{4}3m$) takes place in the film. The phase with the *B*3 structure is non-stoichiometric ($PbS_{0.9}$) and can coexist with the *B*1 structure. Meanwhile, it was shown [123] that the lead to sulfur ratio in PbS thin films is stoichiometric (Pb : S = 1 : 1). The statement of Quadri *et al.*[122] about the *B*3 phase is a mistake, because for interpreting the diffraction data, they suggested that some lead atoms in the detected phase occupy sites 4(*b*) with the coordinates (1/2 1/2 1/2); however, there are no such sites in the *B*3 type structure. The structure of PbS films proposed by Quadri *et al.*[122] is cubic and belongs to space group $F\bar{4}3m$ but does not refer to the *B*3 structural type.

In the thin-layer heterostructures, $PbVS_3$, $PbNbS_3$ and $PbTaS_3$, which represent alternating PbS and transition metal disulfide (VS_2, NbS_2 or TaS_2) layers, lead sulfide can have a monoclinic crystal structure (space groups *C*2, *C*2/*m*, *Cm*2*a*).[124 – 127]

Unfortunately, studies into the synthesis and properties of nanostructured PbS with different morphology usually do not include detailed investigation of the crystal structure. The conclusion about the *B*1 type cubic structure of nanostructured PbS is drawn upon visual comparison of the experimental X-ray diffraction spectrum with the standard data for bulk lead sulfide and comparison of the estimated unit cell constant with the unit cell constant of bulk PbS.

Thorough investigations of the crystal structure of PbS nanopowders and nanofilms were carried out after 2008.[93, 94, 96 – 98, 128]

III.1. Crystal structures of nanopowders and quantum dots

Nanocrystalline PbS powders with an average particle size from 100 to 8 nm were studied by X-ray diffraction.[96, 97] The X-ray diffraction patterns showed considerable reflection broadening. The set of reflections was the same for all nanopowders and, as a first approximation, it corresponded to the cubic structure with space group $Fm\bar{3}m$. The structure was refined using models corresponding to *B*1 (Fig. 15 *a*), *B*2, *B*3, *B*16 and $D0_3$ type structures (Fig. 15 *b*) mentioned in the literature. The best agreement between the experimental and calculated X-ray diffraction patterns was achieved for the *B*1 structure. The use of alternative structures such as *B*2, *B*3, *B*16 and $D0_3$ resulted in poorer agreement between experimental and calculated X-ray diffraction patterns. The results of electron microscopy of the particles of PbS nanopowders [97] are consistent with X-ray diffraction data. Thus, the PbS nanopowders have a cubic (space group $Fm\bar{3}m$) *B*1 structure (see Fig. 15 *a*).

Electron diffraction studies of isolated nanoparticles and lead sulfide QDs [21, 22, 60, 90] in combination with high resolution transmission electron microscopy (HRTEM) confirmed their cubic structure. However, a special quantitative refinement of the crystal structure of PbS quantum dots was never carried out; therefore, the assignment of *B*1 type structure to these objects is hypothetical. Indeed, the crystal structure of PbS nanofilms was also considered to be *B*1, but recent studies demonstrated that this opinion is erroneous.

III.2. Crystal structures of nanofilms

Quantitative determination of the crystal structures of nanostructured PbS films is described in a number of publications.[93, 94, 98, 128]

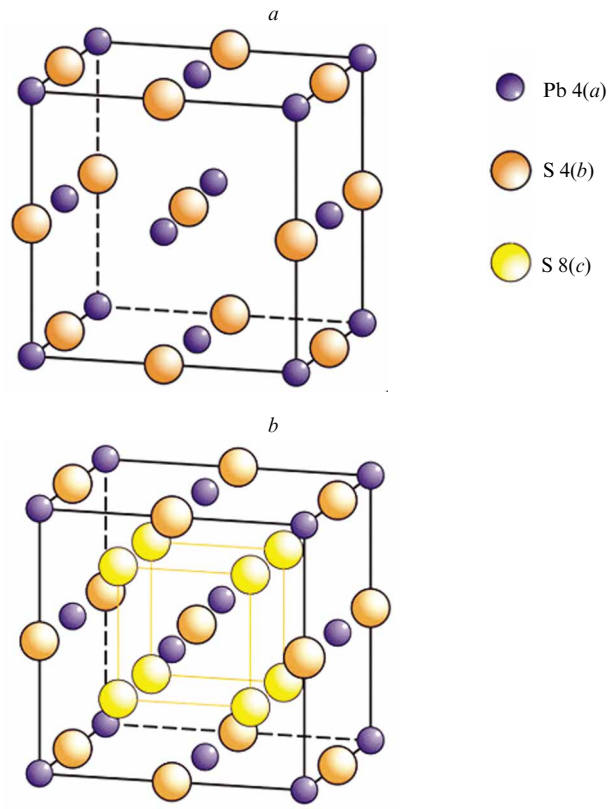


Figure 15. Crystal structures of PbS.
(*a*) Unit cell of coarse-grained cubic (space group $Fm\bar{3}m$) lead sulfide with *B*1 type structure; (*b*) distribution of lead and sulfur atoms in the unit cell of cubic (space group $Fm\bar{3}m$) $D0_3$ structure of a PbS nanofilm.
In the unit cell of the $D0_3$ type structure, sulfur atoms randomly occupy, with probability y, octahedral sites 4(*b*) and randomly occupy, with probability $(1-y)$, tetrahedral sites 8(*c*).

Lead sulfide films of ~100 nm thickness were annealed in air at temperatures from 293 to 423 K with a step of 30–40 K. X-Ray diffraction examination of the films was carried out *in situ* on a Philips X'Pert automated diffractometer equipped with a position-sensitive fast X'Celerator sector detector.

The experimental reflections of the films were markedly broadened. Since the structural type of PbS films has not been unambiguously determined, the authors[93, 94, 98, 128] carried out quantitative analysis of the measured X-ray diffraction patterns using various cubic structure models. The following crystal structure models were considered: cubic *B*1 (space group $Fm\bar{3}m$); cubic *B*3 (space group $F\bar{4}3m$); and a two-phase model of a film in which the relative contents of phases with *B*1 and *B*3 type structures are y and $(1-y)$, respectively. The structure models were evaluated using the Rietveld reliability factor.[129] The minimization of the X-ray diffraction patterns in the two-phase film approximation gave $y = 0.90 \pm 0.02$ and a better reliability factor ($R_{I(B1+B3)} = 0.04$) than the minimization in the one-phase film approximation with either *B*1 or *B*3 type structure ($R_{I(B1)} = 0.05$ and $R_{I(B3)} = 0.12$, respectively). From minimization in the two-phase film approximation, it follows that the lattice constants of *B*1 and *B* 3 phases are equal. From the physical standpoint, this means that the PbS film is a single phase but its structure is not *B*1 or *B*3 type, although it is similar to them.

Sadovnikov *et al.*[93] assumed that the real structure of PbS films corresponds to space group $Fm\bar{3}m$ but the sulfur atoms in it occupy not only octahedral [sites 4(*b*)] but also tetrahedral interstices [sites 8(*c*)] (see Fig. 15 *b*). In this structure, the probabilities for sulfur atoms to occupy sites 4(*b*) and 8(*c*) are equal to y and $(1-y)/2$, respectively. Minimization of the experimental X-ray diffraction patterns of PbS films demonstrated that at any temperature from 293 to 423 K, sites 4(*b*) and 8(*c*) are occupied by sulfur atoms with probabilities of ~0.84 and ~0.08. The reliability factor R_I for all X-ray diffraction patterns did not exceed 0.017. Thus, the crystal lattice of PbS films is characterized by a latent non-stoichiometric distribution of sulfur atoms among sites 4(*b*) and 8(*c*). The new cubic structure (space group $Fm\bar{3}m$) found in the lead sulfide nanofilms corresponds to the $D0_3$ structural type with partially disordered (random) distribution of sulfur atoms over the sites of two types. Considering the crystal structure of nanofilms and the occupancies of sites 4(*b*) and 8(*c*), the formula of the lead sulfide can be written as $Pb^{4(b)}_{0.84}S^{8(c)}_{0.16}$ or $Pb(S_{0.84}\square_{0.16})^{4(b)}(S_{0.16}\square_{0.84})^{8(c)}$, where $\square$ is a structural vacancy.

Sadovnikov and Rempel[130] studied the distribution of the sulfur atoms and vacancies in the square (001) and hexagonal (111) planes formed by sites 4(*b*) and 8(*c*) in the nonmetal sublattice of the nanocrystalline PbS films with cubic $D0_3$ structure and latent non-stoichiometry.

Previously, there was no experimental evidence for the occupation of tetrahedral sites in cubic sulfides by sulfur atoms, and the latent non-stoichiometry of lead sulfide was found for the first time in the studies considered above.[93, 98, 128]

In the cubic structure (space group $Fm\bar{3}m$) of PbS, the radii of the octahedral and tetrahedral interstices are

$$r_{\text{octa}} = \frac{a}{2} - r_{Pb^{2+}} \tag{9}$$

$$r_{\text{tetra}} = \frac{a\sqrt{3}}{4} - r_{Pb^{2+}} \tag{10}$$

The lattice constant a of the PbS films is 0.5940 nm, and the radii of the Pb^{2+} and S^{2-} ions are 0.121 and 0.184 nm, respectively. Therefore, the radii of the octahedral and tetrahedral interstices are ~0.176 and ~0.136 nm, respectively. Since $r_{S^{2-}} > r_{\text{tetra}}$, the location of the S^{2-} anion in the tetrahedral interstice would result in considerable displacements of the nearest lead atoms, which was actually observed in experiments: the microstrains in the films were 0.20% –0.30% at any annealing temperatures up to 423 K.

The occupation of sites 4(*b*) and 8(*c*) by sulfur atoms with the probabilities of ~0.84 and ~0.08, respectively, implies that out of every twelve octahedral interstices, approximately ten are occupied by sulfur atoms and two are vacant. The cubic structure with space group $Fm\bar{3}m$ has twice more tetrahedral interstices than octahedral ones. Therefore, there are 24 tetrahedral interstices per 12 octahedral ones; of these, two are occupied by sulfur atoms and the other are vacant. The absence of superstructural reflections means that the arrangement of sulfur atoms in each type of sites is disordered (random). This is illustrated in Fig. 16, which shows the model of the cubic structure of a PbS film in comparison with the *B*1 structure. The arrange-

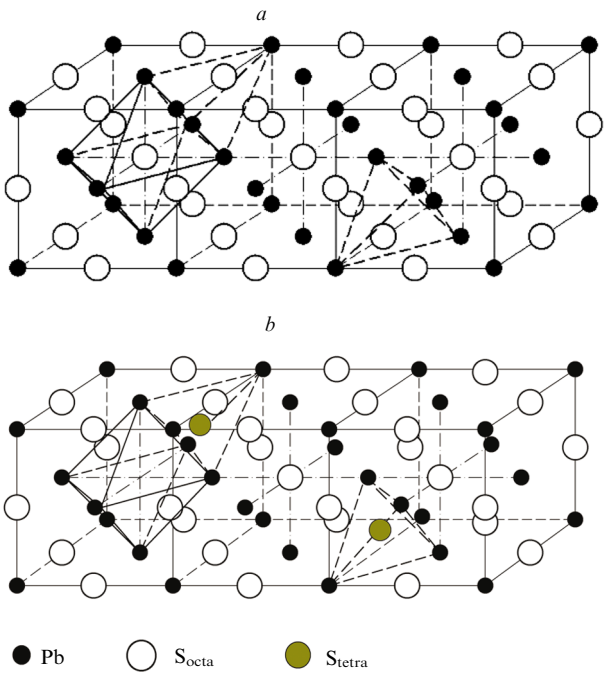


Figure 16. Cubic (space group $Fm\bar{3}m$) $B1$ type structure of lead sulfide (*a*) and a model of the cubic (space group $Fm\bar{3}m$) $D0_3$ type structure of a PbS nanofilm (*b*) with random distribution of sulfur atoms in the octahedral and tetrahedral interstices.[93]

ment of some sulfur atoms in tetrahedral interstices entails some increase in the lattice constant in comparison with the lattice constant of lead sulfide with the $B1$ structure and gives rise to microstrains. As can be seen in Fig. 16, when a sulfur atom occupies a tetrahedral interstice, at least one neighbouring octahedral interstice is vacant, *i.e.*, the crystal lattice of the cubic phase in question has some short-range order.

IV. Properties of nanostructured lead sulfide

Lead sulfide is used in fire alarm sensors and flame sensors, IR detectors and heat source detection systems, photodetectors operating in the range from infrared to ultraviolet, converters of solar energy to electrical energy and other thermoelectric transducers and optical switches. These applications are dependent on the optical and thermal properties of lead sulfide. These properties are briefly considered below.

IV.1. Optical properties and band gap

Of most interest are the properties of nanostructured lead sulfide related to the band gap. There are quite a few publications on the determination of the band gap of PbS as isolated nanoparticles and films.

The first measurements of light transmission and reflection and studies of the absorption edge for PbS films were carried out in the period from 1948 to the 1970s. According to the results of these studies, which were surveyed in a number of publications,[131 – 134] at a temperature of 300 K, the direct band gaps in the single crystalline PbS and in polycrystalline PbS films are 0.41 and 0.42 eV, respectively.

Light scattering and absorption by nanoparticles have specific features and differ from those of coarse-grained materials. For this reason, investigations of size effects in the optical and luminescent properties of semiconductors have attracted considerable attention in recent years.

Electronic excitation of semiconductor crystals gives rise to loosely bound electron – hole pair — an exciton. The exciton delocalization area can be much larger than the crystal lattice constant of the semiconductor; therefore, the decrease in the semiconductor crystal size to a value comparable with the exciton radius affects the properties of the crystal.[5, 8 – 10, 135] For example, as the PbS particle size decreases to 5 nm, the band gap in the electronic spectrum can increase from 0.41 to 1.92 eV (see Refs 55 and 136) or to 2.30 eV.[137] For films based on PbS nanoparticles, the band gap can increase to 2.81 eV.[138] A decrease in the semiconductor particle size should be accompanied by a shift of the absorption band to higher frequency (hypsochromic shift).[139, 140] In the case of lead sulfide films, this shift of the absorption band is observed at a film thickness of <150 nm.[141 – 143]

The recombination of charges generated under the action of light (photons with energy exceeding the band gap) gives rise to luminescence. A hypsochromic shift following a decrease in the particle size was also found in the luminescence spectra of PbS nanoparticles.[113, 138, 144, 145]

Systematic investigations of optical transmission of PbS nanofilms have been reported.[95, 98, 146] The optical transmission spectra were measured for PbS-1, PbS-2, PbS-3 and PbS-4 films and for the PbS-1 film annealed at temperatures of 473 and 523 K (see Fig. 12).

For determining the band gap, most useful is the part of the optical spectra in which the transmittance changes noticeably as a function of wavelength, *i.e.*, the region from 700 – 800 to 2500 – 600 nm corresponding to the photon energies from $\sim$1.6 to $\sim$0.5 eV. In order to quantitatively estimate E_g, absorption spectra rather than transmission spectra are considered. The absorption coefficient (σ) † is the absorbance for a 1 cm thick material layer,

$$\sigma = -\frac{\log T}{s} \tag{11}$$

where $T = I/I_0$ is transmittance in relative units, s is the material thickness, cm.

The spectral dependence of the absorption coefficient $\sigma(\omega)$ on the semiconductor band gap (or the Tauc function) has the form [134, 147 – 149]

$$[\sigma(\omega)\hbar\omega]^{1/n} = A_n(\hbar\omega - E_g) \tag{12}$$

where $\omega = 2\pi c/\lambda$ is the incident radiation frequency; $\hbar\omega = 2\pi\hbar c/\lambda = hc/\lambda$ is the photon energy, A_n is a coefficient independent of frequency ω but depending on the type of transition; the exponent $n = 1/2$ for the direct allowed transition; $n = 3/2$ for the direct forbidden transition; $n = 2$ for the indirect allowed transition; and $n = 3$ for the indirect forbidden transition. When reflection spectra are measured, the $\sigma(\omega)$ value in relation (12) is replaced by the reflection function

† In some publications, this coefficient is designated by α.

$$F(R_\infty) = \frac{(1-R)^2}{2R} \tag{13}$$

defined *via* the reflection coefficient R.

For the direct allowed transitions with $n = 1/2$, relation (12) has the form

$$[\sigma(\omega)\hbar\omega]^2 = A(\hbar\omega - E_g) \tag{14}$$

This equation is more convenient for the quantitative processing of experimental optical absorption data and band gap determination. In an ideal case, $\sigma(\omega) \geqslant 0$ only when $\hbar\omega \geqslant E_g$, and the experimental results in the $[\sigma(\omega)\hbar\omega]^2 - \hbar\omega$ coordinates are described by a linear plot. In a real experiment, since the absorption band is diffuse, the dependence $[\sigma(\omega)\hbar\omega]^2 = f(\hbar\omega)$ is non-linear near the absorption edge; therefore, the band gap is determined as the intercept on the $\hbar\omega$ axis tangential to the linear part of the experimental absorption curve.

Relation (14) was derived without taking account of the electron – hole interaction, which may be significant if the difference $(\hbar\omega - E_g)$ is not too high. The spectral dependence of absorbance derived taking account of the electron – hole interaction has the form [150]

$$\sigma(\omega) = \frac{B}{1 - \exp\left[-C\left(\hbar\omega - E_g\right)^{-1/2}\right]} \tag{15}$$

where B and C are constants. In lead sulfide, the electron – hole interaction is markedly shielded because of the high dielectric constant ε [at 300 K, the ε_{PbS} value varies from 17.2 to 17.9 (see Ref. 133)]; therefore, the absorbance of PbS at $n = 1/2$ is better described by relation (14).

Usually, the films are not monodisperse. Considering this fact, Sadovnikov *et al.*[95] proposed a model for the absorption spectra of polydisperse films. The absorption spectrum of monodisperse nanoparticles is a smooth function of the wavelength or energy ($E = hc/\lambda$). In the case of polydisperse films, the absorption spectra represent superpositions of the spectra corresponding to nanoparticles of different size,

$$\sigma(\omega) = \sum_i c_i \sigma_i(\omega) = \tag{16}$$
$$= \sum_i \frac{c_i A(\hbar\omega - E_{g_i})^{1/2}}{\hbar\omega} \equiv \sum_i \frac{c_i A(E - E_{g_i})^{1/2}}{E}$$

where c_i and E_{gi} are the relative content of nanoparticles of a definite size in the film and the band gap corresponding to these nanoparticles. In polydisperse films, any section of the dependence $[\sigma(\omega)\hbar\omega]^2 \equiv [\sigma E]^2$ is a superposition of $[\sigma_i(\omega)\hbar\omega]^2 \equiv [\sigma_i E]^2$ values; therefore, the observed band gap $E_{g\Sigma}$ is an additive function of the energies E_{gi} corresponding to nanoparticles of different size. Considering the identity

$$[\sigma E]^2 \equiv A^2(E - E_{g\Sigma}) \tag{17}$$

it was approximately shown [95] that

$$E_{g\Sigma} \sim \sum_i c_i^2 E_{g_i} + 2\sum_{i\neq j} c_i c_j (E_{g_i} E_{g_j})^{1/2} + \frac{|E_{g_i} - E_{g_j}|}{3} \tag{18}$$

For a monodisperse film, *i.e.*, when $c_1 = 1$ and $c_{i\neq 1} = 0$, relation (18) is transformed to the obvious boundary condition $E_{g\Sigma} \equiv E_{g1}$.

An important feature of continuous films is the existence of developed grain boundaries. This results in diffuse positions of the conduction and valence bands in the electronic structures of particular grains and, as a consequence, in some uncertainty of the band gap and in additional smearing of the optical spectra of the films. This effect is of the same order as the presence of different size nanoparticles in the film, *i.e.*, the size inhomogeneity of the film, as indicated by Mittleman *et al.*[151]

Thus, the intricate pattern of the absorption spectra of semiconductor films is a consequence of polydispersity.

The absorption spectra of lead sulfide nanofilms plotted in the $[\sigma(\omega)\hbar\omega]^2 - \hbar\omega$ coordinates are shown in Fig. 17. Two (PbS-1 and PbS-4) or three (PbS-2 and PbS-3) linear segments can be distinguished in the spectra. More detailed analysis of the plots for $[\sigma(\omega)\hbar\omega]^2$ revealed a non-monotonic variation of the absorption of PbS-2 and PbS-3 films (see insets in Fig. 17) in the energy region $\hbar\omega = 0.4 - 1.1$ eV; no specific behaviour of absorption was found in this region for PbS-1 and PbS-4 films.

The low-energy absorption edge of all spectra is smeared. The 'tails' observed near the absorption edge, *i.e.*, in the region $\hbar\omega < E_g = 0.41$ eV, are mainly caused by the dispersion (deviation from the mean value) of the size of the film nanoparticles, *i.e.*, inhomogeneous broadening.[151] Other possible causes for absorption edge smearing are structure defects of the semiconductor and/or indirect interband transitions.

The quantitative minimization of the experimental data with respect to absorption coefficient $\sigma(\omega)$ of the PbS-1, PbS-2, PbS-3 and PbS-4 films by function (14) made it possible to find E_g for these films. The calculation showed

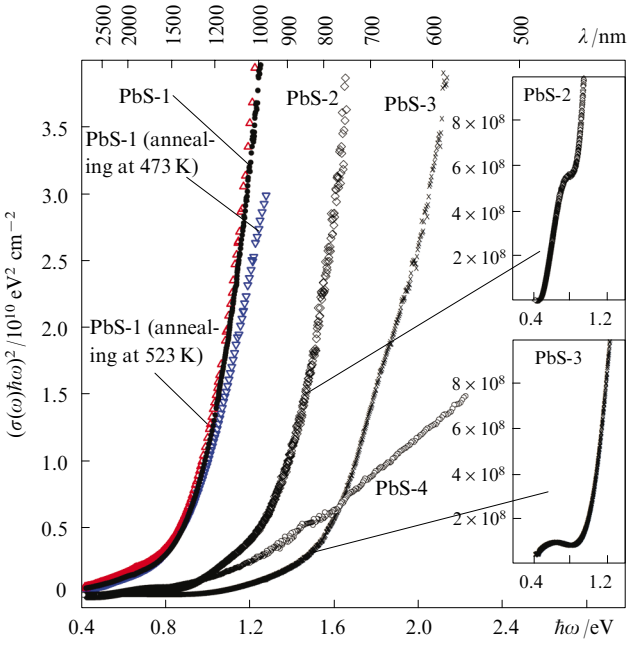


Figure 17. Absorption spectra of PbS films.[95,98]
The insets show the non-monotonic variation of the absorption of PbS-2 and PbS-3 films in the energy range $\hbar\omega = 0.4 - 1.1$ eV.

that the band gap of the synthesized PbS-1 film is 0.92 eV, while the band gaps of the same film after annealing at 473 and 523 K are 0.87 and 0.89 eV, respectively. The average nanoparticle size in the annealed PbS-1 films is 80 nm. For the synthesized and annealed PbS-1 films, the spectral regions with $E < 0.7$ eV are characterized by $E_g \approx 0.42$ eV.

The $[\sigma(\omega)\hbar\omega]^2 = f(\hbar\omega)$ plots for the PbS-2 and PbS-3 films (see Fig. 17) have clear-cut singular points, and between these points, linear segments can be distinguished. For the PbS film, these segments are characterized by the following E_g values:

Film	PbS-2	PbS-3	PbS-4
E_g/eV	~0.43, 0.84, 1.30	~0.98, 1.50	0.41, 1.05

A correlation of the E_g values with the particle size distribution in the PbS films demonstrated that all films contain up to 50% particles with the size from 20 – 100 to 300 nm and more. Apparently, the band gap of these large particles is equal to $E_g = 0.41$ eV characteristic of the coarse-grained lead sulfide.

A considerable contribution to the absorption spectra is made by the groups of nanoparticles corresponding to the maxima of size distributions and the adjacent smaller nanoparticles.[95, 98] In the PbS-1 film, the distribution maximum corresponds to 70 nm particles, and 40% of all particles in the film have a size from 10 to 70 nm; the average nanoparticle size of the PbS-1 film in this range is 60 nm. This average size can be correlated to the E_g value, which was found to be 0.92 eV. In the annealed PbS-1 films, the nanoparticles have an average size of 80 nm and are characterized by $E_g = 0.87 – 0.89$ eV. Size distribution maxima corresponding to nanoparticles of 40 and 70 nm average sizes are inherent in the PbS-2 film. This nanoparticle size can be correlated to the E_g values of 1.30 and 0.84 eV, respectively. The size distribution of particles of the PbS-3 film has two maxima, the average particle sizes at these maxima being 35 and 60 nm. The nanoparticles of these sizes are characterized by E_g values found to be 1.50 and 0.98 eV, respectively. For the PbS-4 film, the weakly pronounced distribution maximum corresponds to an average particle size of 50 nm for which $E_g = 1.05$ eV.

The established correlation between the nanoparticle size in the films and the band gap can serve to elucidate the influence of the PbS nanoparticle size on the E_g value. The E_g value tends to increase as the nanoparticle size decreases (Fig. 18). The band gap of coarse-grained lead sulfide (E_b) is 0.41 – 0.42 eV,[132, 133] and E_g of the considered films[95, 98] increases from $\sim 0.8 \pm 0.1$ to 1.5 ± 0.1 eV as the average nanoparticle size decreases from 80 to 35 nm. In view of this, one can consider that a hypsochromic shift of the optical absorption band was observed in Refs 95 and 98 for PbS nanofilms. The value $E_g = 2.0 \pm 0.1$ eV, similar to the cited results,[95, 98] was found in another paper [152] for PbS films with an average particle size of 40 nm deposited on a glass substrate.

According to the results of Brus,[139] for monodisperse semiconductor nanoparticles, the dependence of the exciton energy (E) on the particle radius ($R = D/2$) is described as

$$E = E_b - \frac{\mu_{ex} e^4}{2n^2\hbar^2} + \frac{n^2\pi^2\hbar^2}{2\mu_{ex}R^2} - \frac{1.78e^2}{\varepsilon R} \quad (19)$$

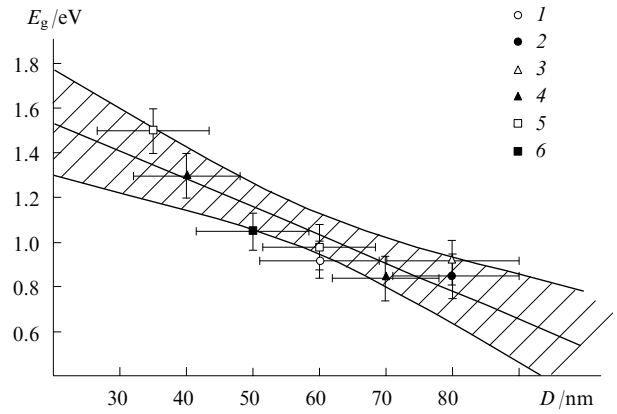


Figure 18. Variation of the band gap *vs.* nanoparticle size in PbS nanofilms.[98]
(*1*) Synthesized PbS-1 film; (*2*) and (*3*) PbS-1 film annealed at 473 and 523 K, respectively; (*4*) – (*6*) PbS-2, PbS-3 and PbS-4 films, respectively. The dashes restrict the 95% confidence range of determination of E_g as a function of particle size.

where $n = 1, 2, 3, \ldots$. In relation (19), the first and second terms are the band gap of the bulk crystal and the electron and hole binding energy (effective Rydberg energy). For coarse-grained lead sulfide, $E_b = 0.41 – 0.42$ eV. The third term is the exciton kinetic energy, and the last term takes into account the Coulomb interaction between an electron and a hole. Thus, interband absorption should give rise to a series of discrete lines for different n values and the absorption threshold is determined by transition to the ground state with $n = 1$. The sum of the first, third and fourth terms of Eqn (19) is the effective band gap; for the ground state ($n = 1$), it is expressed as

$$E_g(R) = E_b + \frac{\pi^2\hbar^2}{2\mu_{ex}R^2} - \frac{1.78e^2}{\varepsilon R} \quad (20)$$

For lead sulfide with the particle size $D \geqslant 10$ nm, the correction for Coulomb interaction is lower, ~0.029 eV (~7% of the value $E_b = 0.41 – 0.42$ eV typical of coarse-grained PbS); therefore, in the first approximation, this correction in Eqn (20) can be neglected. Then the dependence of E_g on the particle radius is described by the relation

$$E_g = E_b + \frac{\pi^2\hbar^2}{2\mu_{ex}R^2} \quad (21)$$

which means that

$$E_g(R) \propto \frac{1}{R^2} \quad (22)$$

or

$$E_g(D) \propto \frac{1}{D^2} \quad (23)$$

In the optical properties of semiconductors, the size effects are manifested most clearly if the particle size is commensurable with (or less than) the characteristic size of the Wannier – Mott exciton

$$R_{ex} = a_B \frac{n^2\varepsilon m_0}{m_{ex}} \quad (24)$$

where $a_B = \hbar^2/m_0e^2 = 0.053$ nm is the Bohr radius. A pronounced localization is best achievable for narrow-band-gap semiconductors with a high dielectric constant; this weakens considerably the electron – hole electrostatic interaction and, as a result, the exciton radius increases (the exciton size may far exceed the crystal lattice constant). The electron and hole effective masses, respectively, for lead sulfide at 4 K are given by [153]

$$m_e = (0.092 \pm 0.012)m_0 \quad (25)$$

$$m_h = (0.090 \pm 0.015)m_0 \quad (26)$$

therefore, the exciton mass

$$\mu_{ex} = (0.045 \pm 0.006)m_0 \quad (27)$$

For this μ_{ex} value and the dielectric constant $\varepsilon_{PbS} \approx 18$ for lead disulfide,[133, 153] the radius R_{ex} of the first exciton state with $n = 1$ is $(22 \pm 3)\varepsilon a_B$ or 18–4 nm.

Despite the fact that the average PbS particle size in the films studied by Sadovnikov *et al.*[95, 98] and Kumar *et al.*[152] is 2–4 times as large as the exciton size, the band gap is much wider than that in the bulk coarse-grained PbS. This is due to the considerable dispersion of nanoparticle sizes: the presence of particles smaller than ~10–30 nm in the films accounts for the increase in the band gap, while the presence of much larger particles leads to the average particle size increasing to ~60–80 nm.[95, 98]

The band gap found for the isolated PbS particles which were dispersed in a polymeric film matrix (Fig. 19) is, most often, greater than E_g of nanofilms (see Fig. 17). According to Jana *et al.*,[138] the E_g values for 8, 12 and 18 nm nanoparticles are 2.81, 2.62 and 2.40 eV, respectively. The isolated PbS nanoparticles of ~ 13 nm size distributed in a copolymer matrix have $E_g = 3.36$ eV.[154] For isolated PbS particles of 1.5 to 12.5 nm size dispersed in a polymeric film matrix, E_g was found to be from 2.4 to 0.5 eV.[155] However, the size of PbS nanoparticles in the cited paper[155] is apparently underestimated. In the case of 0.8 to 2.8 nm

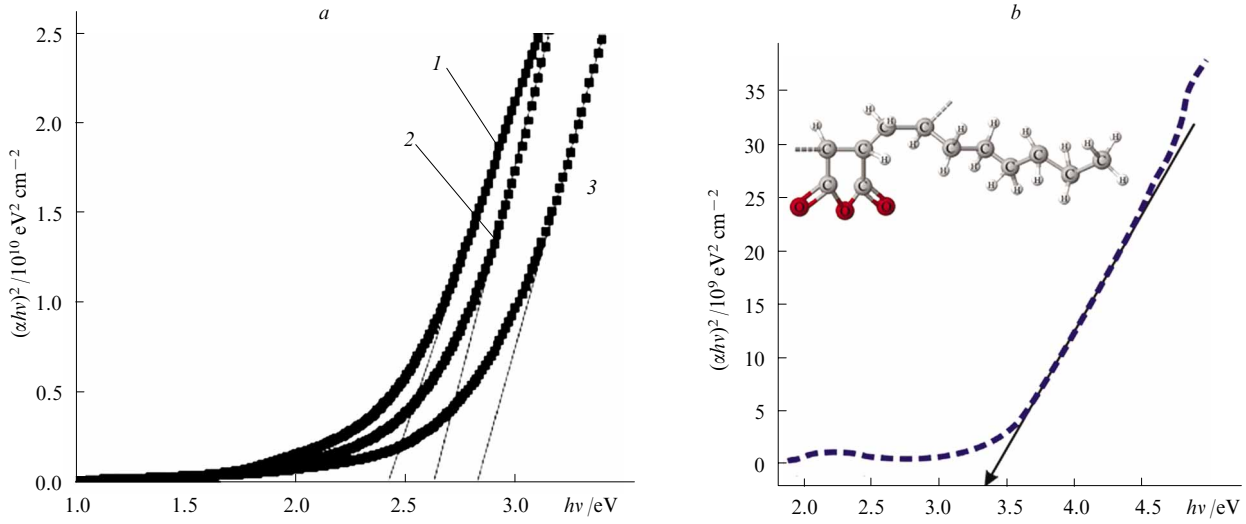


Figure 19. Absorption spectra and band gap of isolated PbS nanoparticles.
(*a*) Polyvinyl alcohol matrix; the deposition temperatures for 18 (*1*), 12 (*2*) and 8 nm (*3*) particles are 303, 293 and 283 K, respectively;[138] (*b*) copolymer matrix with PbS nanoparticles of ~13 nm size; the inset shows the presumptive molecular structure of the copolymer.[154]

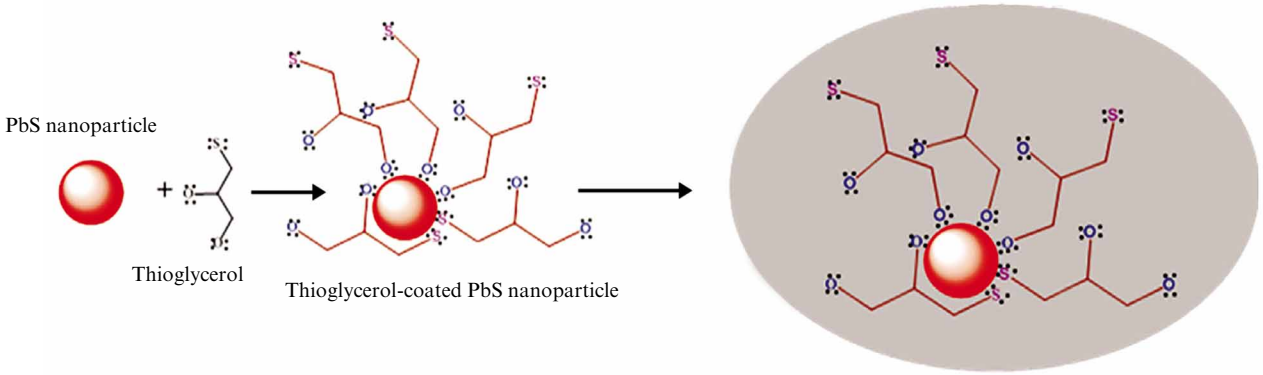


Figure 20. Mechanism of formation of thioglycerol-coated PbS nanoparticles in a polyvinyl alcohol matrix.[157]

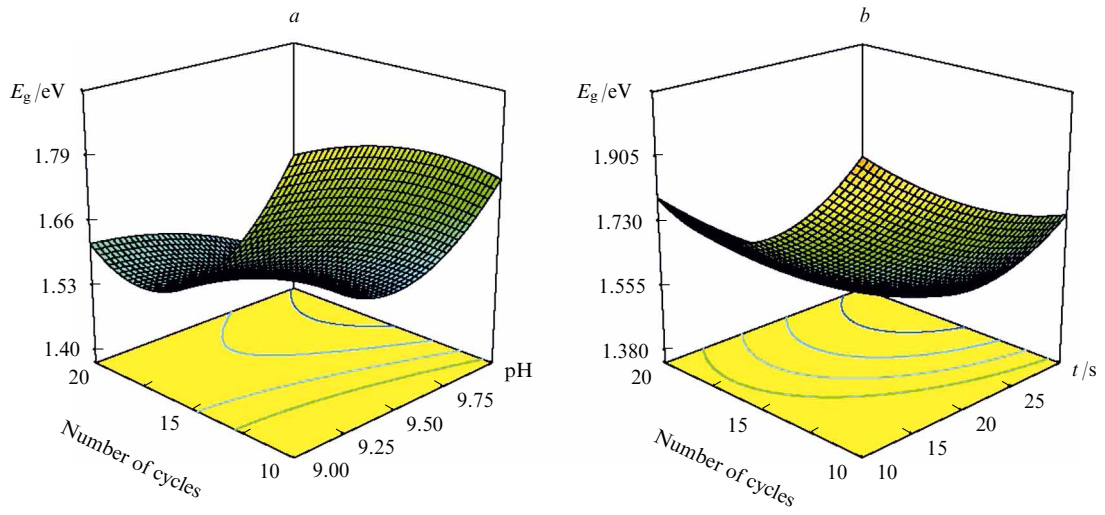


Figure 21. Band gap of PbS films obtained by the SILAR process *vs.* pH of the reaction mixture (*a*), duration (*b*) and number of dipping cycles of the substrate into the reaction mixture (*a*, *b*).[109]

PbS nanoparticles dispersed in a polyacrylamide film, the absorption band shifts hypsochromically to 2.6 – 2.8 eV.[156] An E_g value of 3.76 eV was reported for isolated PbS nanoparticles not exceeding 15 nm size coated by thioglycerol and dispersed in polyvinyl alcohol [157] (Fig. 20). According to Chakraborty and Moulik,[23] colloidal PbS nanoparticles of 2.4 to 3.0 nm size synthesized in an aqueous heptane microemulsion are characterized by E_g ranging from 3.45 to 3.30 eV.

Yucel *et al.*[109] determined the band gap of nanostructured PbS films prepared on a glass substrate by the SILAR process. Deposition was performed from a mixture of 1 M aqueous solutions of lead acetate and sodium sulfide at room temperature. The E_g value was found as a function of conditions of synthesis [pH and the number and time (t) of cycles of substrate dipping into the reaction medium] (Fig. 21). According to the study of Yucel *et al.*,[109] a PbS film with the greatest band gap of 2.24 eV can be synthesized by the SILAR method at pH 9.1 using ten dipping cycles, 10 s each.

IV.2. Thermal properties

Data on the thermal expansion of lead sulfide, including films, are very scarce, although these data are useful for the application of films at elevated temperature and for selection of substrates with similar thermal expansion coefficients. It was found [158, 159] that the thermal expansion coefficient of polycrystalline PbS at 300 K is (19 – 20) 10^{-6} K^{-1}. According to one publication,[159] the Grüneisen constant (γ) of polycrystalline PbS monotonically decreases from ~2.2 to ~1.9 as the temperature is raised from 20 to 340 K, while according to the other mentioned paper,[158] the constant γ, conversely, increases from 1.98 to 2.26 with temperature rise from 320 to 670 K. The lattice properties of PbS were calculated by *ab initio* density functional theory in the quasiharmonic approximation.[160] At 300 K, the thermal expansion coefficient (α) and the Grüneisen constant of lead sulfide were found to be 29.8 10^6 K^{-1} and 2.50 – 2.52, respectively.[160]

The thermal expansion coefficient of a nanostructured PbS film has been measured by Sadovnikov *et al.*[94, 161] According to one study,[94] as the PbS film is cooled down from 423 to 293 K, the lattice constant a decreases from 0.59637 to 0.59326 nm, and this change in the lattice constant is correlated with the thermal expansion coefficient $\alpha(423\ K) \approx 40 \times 10^{-6}\ K^{-1}$. Upon the repeated heating of the PbS film from 293 to 393 K, the lattice constant increases from 0.59326 to 0.59492 nm. This change implies that $\alpha(393\ K) \approx 28 \times 10^{-6}\ K^{-1}$.

The first study of the thermal expansion of the PbS nanofilm *in situ* at temperatures of up to 443 K was reported by Sadovnikov *et al.*[161] The measured linear thermal expansion coefficient of the PbS nanofilm was $(37-39) \times 10^{-6}\ K^{-1}$, which is close to the value α determined in another publication.[94] Note that the presented α value of nanofilms is approximately twice as high as α of the coarse-grained PbS. The researchers cited [161] stated, without discussing the physical grounds of the observed effect, that the great difference between the coefficients α is attributable to the small particle size of PbS in the films and to different crystal structures of the films and coarse-grained PbS.

The precise diffraction measurements of the films [161] were carried out *in situ* at temperatures from 293 to 473 K on a Philips X'Pert automated diffractometer equipped with a position-sensitive fast X'Celerator sector detector. The error of determination of the lattice constant did not exceed ± 0.00005 nm.

The structure refinement of the PbS film demonstrated[161] that reflection positions and intensities correspond to cubic (space group $Fm\bar{3}m$) lead sulfide with $D0_3$ type structure, which is in line with the results of other publications.[93, 94, 98] The crystal lattice constant a_{cub} of the PbS film is 0.59335 ± 0.00005 nm; all of the observed diffraction reflections were substantially broadened. An estimation showed that the average coherent scattering region (CSR) in the film is ~40 nm.

According to the results of measurements,[161] the dependence of the lattice constant a on the annealing temperature T is non-linear and in the range of 293 – 473 K, it is described by the polynomial

$$a(T) = a_0 + a_1 T + a_2 T^2 + a_3 T^3 \qquad (28)$$

where $a_0 = 0.59057$ nm, $a_1 = -8.1896 \times 10^{-6}$ nm K^{-1}, $a_2 = 7.9452 \times 10^{-8}$ nm K^{-2} and $a_3 = -6.5455 \times 10^{-11}$ nm K^{-3}. The dependence of α on the annealing temperature in the range of 323–473 K can be represented in terms of the coefficients of polynomial (28) as

$$\alpha(T) = \frac{(a_1 + A_2 T = a_3 T_0^2) + (a_2 + a_3 T_0)T + a_3 T^2}{a_{293\mathrm{K}}} = \quad (29)$$

$$= 9.4705 \times 10^{-6} + 6.0273 \times 10^{-8} T - 6.5455 \times 10^{-11} T^2$$

On the time scale of performed experiments,[161] the relaxation processes in the PbS nanofilm were very slow, and the equilibrium values of the lattice constant a and the thermal expansion coefficient were achieved only after many-hour annealing. The measured thermal expansion coefficient of the PbS nanofilm was much higher than that reported in the literature [158–160] for bulk PbS.

The difference between the coefficients α of nanofilms and bulk coarse-grained PbS can be caused by the following reasons:[162, 163]

— substrate effect;

— method of measurement;

— different crystal structures;

— small particle size in the nanofilm, which results in a change in the phonon spectrum and its boundaries.

The thermal expansion coefficient of the glass substrate in the temperature range of 293–473 K measured by dilatometry [161] was 12.5×10^{-6} K^{-1}, which was three times as low as the α value of the PbS nanofilm. Therefore, the effect of the substrate on α_{PbS} can be ruled out. Different methods of measurement of the thermal expansion coefficient used in the cited studies [158, 159, 161] may be responsible for the difference between the coefficients α but by not more than 5%. Thus, the main reasons for the difference between the coefficients α of nanofilms and bulk PbS are their different crystal structures ($D0_3$ type for nanofilms and $B1$ for bulk PbS) and a small particle size in the nanofilm.

A decrease in the size of particles (grains, crystallites) to the nanometre range is known to be accompanied by increase in the thermal expansion coefficient compared with α of conventional polycrystals.[9, 10] Exactly this effect was observed by Sadovnikov *et al.*[161] and explained in other publications.[162, 163]

The thermal expansion of a solid is caused by anharmonicity of atomic vibrations. In the first approximation, the potential energy of a system of interacting atoms (U) as a function of $u = (r - r_0)$ has the form

$$U(u) = U_0 + \frac{A_h U^2}{2} - \frac{\beta u 3}{3} \quad (30)$$

where

$$A_h = \left(\frac{\partial^2 U}{\partial r^2}\right)_{r=r_0} \quad (31)$$

is a constant, r is the deviation of the atom from the equilibrium position r_0,

$$\beta = \frac{1}{2}\left(\frac{\partial^3 U}{\partial r^3}\right)_{r=r_0} \quad (32)$$

is a coefficient taking account of the anharmonicity of atomic vibrations.

The equation for the linear thermal expansion coefficient has the form

$$\alpha(T) = \left(\frac{1}{a_{293}}\right)\frac{\mathrm{d}\langle u\rangle}{\mathrm{d}T} = \frac{k_{\mathrm{B}}\beta}{A_h^2 a_{293}} \quad (33)$$

where a_{293} is the crystal lattice constant. The thermal expansion (or compression) of a solid can be explained only considering the anharmonicity of atomic vibrations, *i.e.*, when $\beta \neq 0$, because in the harmonic approximation where $\beta = 0$, the linear expansion coefficient is zero and thermal expansion is absent. It is clear from relation (33) that the increase in the thermal expansion coefficient on going from coarse-grained to nanostructured lead sulfide is possible only provided that the coefficient β increases, *i.e.*, if the atomic vibrations are anharmonic.

The linear thermal expansion coefficient $\alpha(T)$ is related to the specific heat capacity referred to unit volume, $C_{\mathrm{sp}} = C_V/v_{\mathrm{m}}$, and measured in J m^{-3} K^{-1} by the following expression:

$$\alpha(T) = \frac{\gamma C_{\mathrm{sp}}(T)}{3B} \equiv \frac{\gamma}{3B}\frac{C_V(T)}{v_{\mathrm{m}}} \quad (34)$$

where B is the triaxial compression module, v_{m} is the molar volume. If the lattice heat capacity C_V of a monoatomic substance is represented in terms of the average linear oscillator energy $\varepsilon(\omega T)$ and the frequency distribution function $g(\omega)$, relation (34) takes the form

$$\alpha(T) = \frac{\gamma}{3v_{\mathrm{m}} B}\int \frac{\partial\varepsilon(\omega, T)}{\partial T} g(\omega)\mathrm{d}\omega \quad (35)$$

It can be seen from Eqn (35) that the temperature dependence of the thermal expansion coefficient depends directly on the spectral frequency distribution $g(\omega)$. Thus, the change in the lattice properties of nanocrystals with respect to analogous properties of bulk coarse-grained samples is mainly caused by a change in the pattern and boundaries of the phonon spectrum, *i.e.*, by the change in the distribution function of the atomic vibration frequencies.

The key idea of most models for modification of the phonon spectrum of small particles and/or nanostructured systems is the appearance of low-frequency modes, which are missing from the spectrum of a bulk coarse-grained sample.[9, 10] According to published data,[9, 164] waves with a wavelength not exceeding twice the largest particle diameter, $\lambda \leqslant 2D$, can be generated in nanoparticles; therefore, on the low-frequency side, the phonon spectrum is restricted by some minimum frequency

$$\omega_{\min} \sim \frac{c_{\mathrm{t}}}{2D} \sim 2\pi\frac{c_{\mathrm{t}}}{2D}\omega_{\min} \geqslant 2\pi\frac{c_{\mathrm{t}}}{2D} \quad (36)$$

where c_{t} is the propagation velocity of transverse elastic vibrations (transverse velocity of sound). There is no such restriction in the bulk crystals. In addition, the phonon spectrum is restricted from higher frequencies.

The distribution of normal modes in the presence of low-frequency restriction and the expressions for the distribution function $g(\omega)$ and the upper boundary $\omega_{\max}$ of the

phonon spectrum of a small rectangular particle were reported by Montroll.[165] Considering these expressions, it was shown [162, 163] that the molar heat capacity of a nanocrystalline material consisting of rectangular particles can be represented as a function of not only the temperature but also the size (D) of a small particle

$$C_V(T, D) = \quad (37)$$

$$= n\left[\frac{12\pi^4 N_A k_B}{5}\left(\frac{k_B T}{\hbar\omega_{max}}\right)^3 + k_1 L_\Sigma T + k_2 S_\Sigma T^2\right] =$$

$$= C_V^{bulk}(T) + n\left(k_1 L_\Sigma T + k_2 S_\Sigma T^2\right)$$

where n is the number of atoms in the molecule. The first term is the Debye heat capacity of the bulk coarse-grained crystal in the low-temperature region; L_Σ and S_Σ are the total edge length and the total surface area of small particles; the coefficients k_1 and k_2 are positive values depending on the elastic constants of the crystal.

Taking account of relations (34) and (37) and the expressions for L_Σ and S_Σ, the thermal expansion coefficient of a nanocrystalline compound can be represented in the form [162, 163]

$$\alpha(T, D) = \frac{\gamma C_V^{bulk}(T)}{3v_m B} + n\frac{\gamma}{3v_m B}\left(k_1 L_\Sigma T + k_2 S_\Sigma T^2\right) = \quad (38)$$

$$= \alpha_{bulk}(T) + n\frac{\gamma}{3B}\left(\frac{12k_1 T}{D^2} + \frac{6k_2 T^2}{D}\right)$$

The contribution to the thermal expansion coefficient caused by the small particle size is

$$\Delta\alpha(T, D) = n\frac{\gamma}{3B}\left(\frac{12k_1 T}{D^2} + \frac{6k_2 T^2}{D}\right) \quad (39)$$

Sadovnikov and Gusev [162, 163] calculated the coefficients k_1 and k_2 using the propagation velocities of longitudinal and transverse elastic vibrations c_l and c_t or elastic constants c_{11}, c_{12} and c_{44} for lead sulfide.[160, 166 – 169]

In highly symmetrical crystals, fully longitudinal or fully transverse atomic vibrations propagate only in those directions that correspond to the planes of synchronously moving atoms. For cubic crystals, these are [100], [110], [111] and other equivalent directions. The calculation [162, 163] using published data [166] demonstrated that the velocities c_l and c_t for PbS at ~300 K are ~3975 and ~1881 m s^{-1}. Changes in the propagation velocities of transverse and longitudinal elastic vibrations depending on the crystallographic direction for a single crystal of cubic PbS at 300 K is illustrated in Fig. 22.

According to estimates carried out with these values, the lower and upper boundaries ω_{min} and ω_{max} of the phonon spectrum of a small cubic PbS particle with 50 nm edges amount to $\sim 1.18\times10^{11}$ and $\sim 2.76\times10^{13}$ rad s^{-1}, respectively.[162, 163] The constants k_1 and k_2 at 300 K are $\sim 1.55\times10^{-16}$ J m^{-1} K^{-2} and $\sim 6.00\times10^{-8}$ J m^{-2} K^{-3}, *i.e.*, $k_2 \gg k_1$. As the temperature increases to 500 K, the constants k_1 and k_2 increase slightly to $\sim 1.67\times10^{-16}$ J m^{-1} K^{-2} and $\sim 7.06\times10^{-8}$ J m^{-2} K^{-3}, respectively. Since $k_2 \geqslant k_1$, it follows from relation (39) that in the case of small particles, an additional contribution proportional to $S_\Sigma T^2$ and induced by the large surface area of small particles appears in the thermal expansion coefficient. Therefore, a decrease in the particle size to a nanometre range should be accompanied by an increase in the thermal expansion coefficient. It is exactly this effect — a ~1.7 times greater α value of a PbS nanofilm than α of a bulk coarse-grained PbS — was observed in the cited studies.[161 – 163]

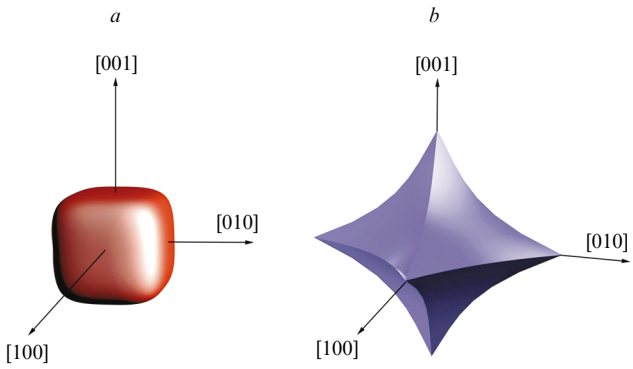


Figure 22. Changes in the propagation velocities of the transverse (*a*) and longitudinal (*b*) elastic vibrations along crystallographic directions in a single crystal of cubic PbS at 300 K.[162]
The distances from the figure centres are proportional to the velocities $c_t^{[100]} = c_t^{[010]} = c_t^{[001]} = 1.9\times10^3$ (*a*) and $c_l^{[100]} = c_l^{[010]} = c_l^{[001]} = 4.0\times10^3$ m s^{-1} (*b*).

The dependence of the thermal expansion coefficient of a PbS nanofilm in the temperature range from 300 to 500 K calculated as

$$\alpha_{nano}^{calc}(T, D) = \alpha_{bulk}(T) + \Delta\alpha(T, D) \quad (40)$$

taking account of the determined coefficients k_1 and k_2 is presented in Fig. 23. As the $\alpha_{bulk}(T)$ dependence, the reported [158] experimental results were used. The calculation

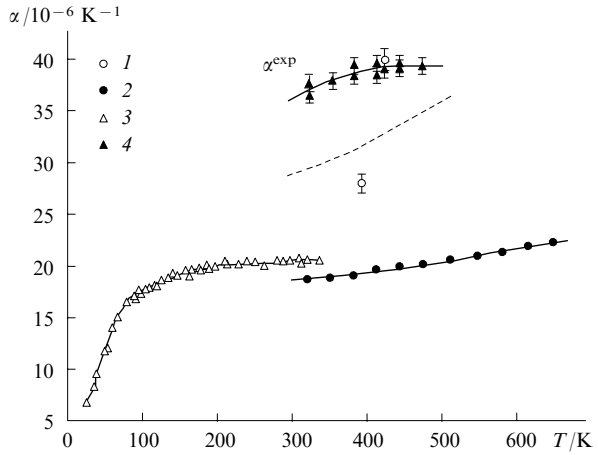


Figure 23. Temperature dependences of the linear thermal expansion coefficient of lead sulfide.
(*1*) PbS nanofilm;[161] (*2*), (*3*) coarse-grained polycrystalline PbS according to Refs 158 and 159, respectively; (*4*) PbS nanofilm.[162]
The dashed line shows the dependence of the thermal expansion coefficient of a PbS nanofilm calculated from Eqn (40).

took into account the temperature variation of the equilibrium particle size in the PbS nanofilm, as well as the slight linear increase in the Grüneisen constant [158] and the decrease in the triaxial compression modulus B [166] with temperature rise. For comparison, Fig. 23 presents the experimental values α values of a PbS nanofilm [161] and reported data for bulk PbS [158, 159] and for films.[162]

The calculated dependence for a PbS nanofilm is located somewhat lower than the experimental plot:[159] in the temperature range of 300–473 K, the difference between the coefficients α is $(5-6)\times10^{-6}$ K^{-1}. Apparently, this is a consequence of the approximations of the model [165] used as the basis for calculations.[162, 163] Furthermore, the experimental data [166] used to estimate the effective propagation velocities of elastic vibrations, c_1^{-1}, c_2^{-1}, c_3^{-1}, and for the subsequent calculation of $\Delta\alpha(T, D)$ as well as the data of Sharma,[158] which were taken as $\alpha_{\text{bulk}}(T)$ for lead sulfide, may not be entirely accurate. Considering these facts, the agreement between the calculated and experimental plots for the thermal expansion coefficient of a PbS nanofilm is quite satisfactory (see Fig. 23).

The thermal expansion coefficient of a PbS film at 423 K estimated from data [94] on the change in the lattice constant on cooling the film from 423 to 293 K amounts to $\sim40\ 10^{-6}$ K^{-1}, which is quite consistent with experimental results.[161] The estimation of α from the data [94] obtained while heating a film from room temperature to 393 K gives a lower value — $\sim28\times10^{-6}$ K^{-1}. This may be caused by the fact that in Ref. 94, the annealing of the PbS film at 393 K was too short for the equilibrium lattice constant to be attained.

Since

$$\beta=\frac{A_h^2 a_{293}\alpha}{k_{\text{B}}} \tag{41}$$

then, taking into account expression (38), the dependence of the atomic vibration anharmonicity factor on the particle size can be represented in the form

$$\beta(T, D)= \tag{42}$$
$$=\frac{A_h^2 a_{293}}{k_{\text{B}}}\left[\alpha_{\text{bulk}}(T)+n\frac{\gamma}{3\nu_{\text{m}}B}\left(k_1 L_\Sigma T+k_2 S_\Sigma T^2\right)\right]$$

According to this equation, a decrease in the particle size, resulting in an increase in the particle surface area (S_Σ), should be accompanied by an increase in the anharmonicity of atomic vibrations.

According to numerous publications,[52, 93–95, 98, 122, 170] the PbS lattice constant remains invariable with a decrease in the particle size. With the assumption that the coefficient A_h also remains the same as the particle size decreases, the ratio of the anharmonicity coefficients of nanofilms and bulk PbS is given by

$$\frac{\beta_{\text{nano}}}{\beta}=\frac{\alpha_{\text{nano}}}{\alpha} \tag{43}$$

hence,

$$\beta_{\text{nano}}=\frac{\alpha_{\text{nano}}}{\alpha}\beta \tag{44}$$

At a temperature of 293 K, the coefficient α of bulk PbS is $\sim21\times10^{-6}$ K^{-1} (see Refs 153 and 159), and the measured thermal expansion coefficient of nanofilms $\alpha_{\text{nano}}\approx36\times10^{-6}$ K^{-1}. Therefore, $\beta_{\text{nano}}\approx1.7$.

Thus, the linear thermal expansion coefficient of a PbS nanofilm in the temperature range of 293–443 K is approximately 1.5 to 2 times as high as the α of bulk PbS. The observed difference between the coefficients α is associated with the small PbS particle size in the film, resulting in a change of the distribution function of the atomic vibration frequencies and an increase in the vibration anharmonicity.

IV.3. Stability of nanostructured lead sulfide

The most widely used devices based on lead sulfide are fire alarm sensors, flame sensors and heat source detection systems;[171, 172] therefore, the thermal and oxidation stabilities of the nanostate largely determine the application of nanostructured PbS in this type of devices. However, nanoparticles and quantum dots are metastable materials and are prone to recrystallization and oxidative degradation, which is promoted by their large specific surface area. Therefore, extensive use of nanostructured PbS requires the knowledge of the temperature range in which the nanoparticles do not grow (no transition from the nano- to the coarse-grained state) and the temperature of the onset of oxidation.

The thermal stability of the structure of PbS nanofilms obtained by laser deposition on heated quartz substrates has been studied.[122] The annealing of films in air demonstrated that upon temperature rise to 375 K, the intensity ratio of some diffraction reflections changes but no additional peaks are observed up to 475 K; hence, the PbS nanofilm is not oxidized. The change in the diffraction reflection intensities was attributed [122] to the fact that a phase transition from the $B1$ structure to the high-temperature cubic $B3$ structure (space group $F\bar{4}3m$) takes place in the PbS film at 375 K.

The thermal stability of lead sulfide nanopowders and nanofilms and their recrystallization in vacuum and oxidation in air are the subjects of several publications.[173–175] The lead sulfide nanopowders with a particle size of 10–20 nm were prepared by deposition from aqueous solutions of lead acetate and sodium sulfide in the presence of Trilon B as a complexing agent. The lead sulfide films on glass substrates were obtained by chemical deposition from aqueous solutions of lead citrate and thiourea. The synthesized PbS nanopowders were annealed under dynamic vacuum of 10^{-3} Pa and in air in the temperature range of 423–930 K with a step of 50 K. The annealing of nanopowders lasted for an hour, and the nanofilms were annealed for 5 h. According to electron microscopy data, when the annealing temperature is raised, agglomeration of particles of PbS powders, together with the particle growth, is observed.

The vacuum annealing of PbS nanopowders at a temperature of up to 700 K leads to minimization of microstrains and a slight growth of nanoparticles (Fig. 24 *a*); hence, this temperature range can be regarded as the thermal stability region of lead sulfide nanopowders. The temperature range from 700 to 800 K, in which the particle size increases 5–10-fold, corresponds to the temperature of accumulative recrystallization of PbS nanopowder. The vacuum annealing of PbS nanofilms at a temperature of up to 673 K is also accompanied by a minor growth of nanocrystallites, while at higher annealing temperature, the particle size increases jumpwise (Fig. 24 *b*). The recrystallization in nanofilms starts at a lower temperature than the recrystallization of nanopowders. This is a consequence of tighter contact of

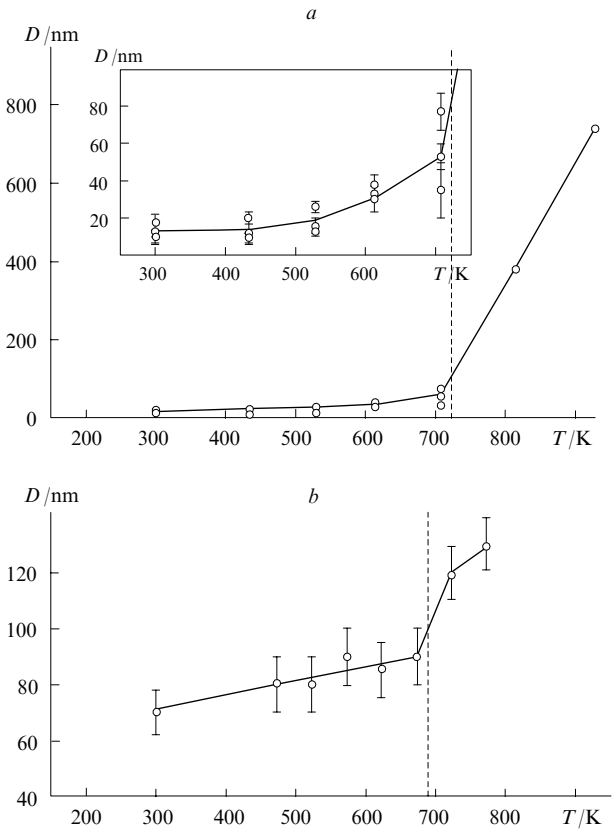


Figure 24. Effect of the vacuum annealing temperature on the particle (crystallite) size in nanostructured PbS powders (*a*) and films (*b*).[173, 174]
The temperature of the onset of recrystallization is marked by the dashed line.

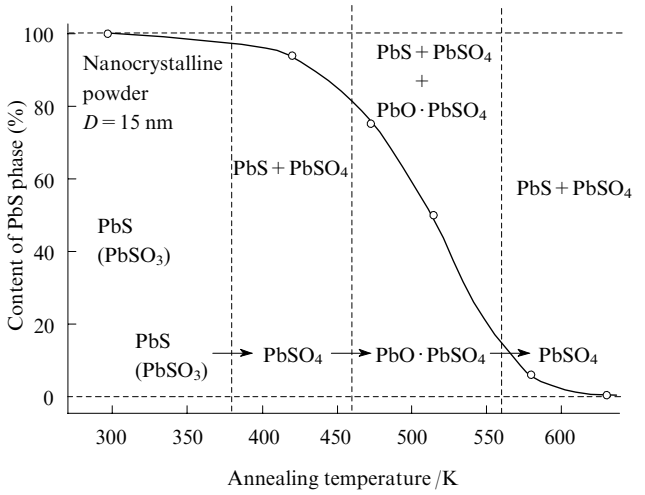


Figure 25. Content of the PbS phase in a PbS nanopowder with a 15 nm particle size *vs.* annealing temperature in air.[174]
A minor amount of $PbSO_3$ is present in the synthesized nanopowder as an impurity. The dashed lines mark the conventional temperatures of transitions from one phase to the other.

crystallites in nanofilms compared with the particle contact in nanopowders.

It was found [10, 176] that accumulative recrystallization in nanocrystalline materials starts, most often, at the temperatures $T_{recr} \approx (0.30-0.35)\,T_m$. In other studies,[173, 174] the recrystallization temperature of PbS nanopowders and nanofilms was found to be $\sim$700 K, which is half the melting point of bulk PbS (1391 K). Thus, PbS nanopowders and nanofilms have higher relative recrystallization temperature $T_{recr} \approx 0.5\,T_m$, *i.e.*, they differ from other nanomaterials by a higher thermal stability of particle (crystallite) size.

Comparative analysis of the oxidative activities of lead sulfide demonstrated that the temperatures of the onset of all oxidative processes are much lower for PbS nanopowders than for the bulk coarse-grained sulfide, these processes being facilitated by oxygen-containing impurities.[174, 175] A decrease in the particle size is accompanied by a shift of the onset of oxidation to lower temperatures, while the oxidation of bulk lead sulfide starts at about 800 K.[177]

The sequence of transformations involved in the oxidation of lead sulfide is illustrated in Fig. 25 in relation to PbS nanopowder with a particle size of 15 nm.[174] The small amount ($\sim$10 mass %) of $PbSO_3$ present in the initial nanopowder has been formed during the PbS synthesis. As the temperature is raised from 423 to 473 K, the amount of $PbSO_3$ first increases and then (on further temperature rise) decreases, and at 573 K, this phase disappears. The absence of PbO in the temperature range of 423 – 623 K indicates that the reactions yielding this oxide as the final product proceed at higher temperature ($>$700 K). The temperature of the onset of oxidation of PbS nanopowders increases with increase in the nanoparticle size.

When PbS nanofilms are annealed in air at temperatures below 623 K, no oxidation takes place. This is consistent with the data of another publication.[122] Annealing at $T > 623$ K leads to partial film oxidation to give the $PbO \cdot PbSO_4$ oxide sulfate phase on the film surface. Thus, the nanostructured film of lead sulfide is stable in air up to 573 K and is more stable against oxidation than nanopowders.[174]

The results obtained by Mikhlin *et al.*[178] are useful for the understanding of the oxidation pattern of nanostructured PbS. According to these results, the surface of a single-crystalline sulfide is oxidized in air only at increased relative humidity reaching $\sim$90%. The oxidation products form $\sim$20-nm protrusions on the PbS surface. Water condensed on the protrusions promotes the oxidation of PbS. Over a period of three to five days, the protrusions uniformly cover the surface and then merge together to form a loose surface oxide layer. At normal or low air humidity, the lead sulfide surface is not oxidized. The oxidation of nanostructured PbS also starts on the surface but at a lower humidity.

According to Ihly *et al.*,[179] keeping PbS quantum dots in air is accompanied by a hypsochromic shift of the first exciton peak in the optical spectra. This shift is caused by partial oxidation of the QDs. Nanostructured films were prepared by layer-by-layer deposition of lead sulfide accomplished by dipping the substrate into a colloidal solution of QDs. The oxidation of PbS nanofilms in air was found to induce broadening of the first exciton peak. In order to prevent the oxidative degradation of nanostructured lead sulfide films, it was proposed to cover the films by an amorphous Al_2O_3 layer. A 18-nm thick Al_2O_3 layer com-

pletely prevents the oxidation of PbS nanofilms and prevents the growth of nanoparticles in the films.

V. Applications of nanostructured lead sulfide

Traditional applications of lead sulfide, in particular nanostructured one, in devices such as broad-band photodetectors, high-efficiency solar cells, thermoelectric transducers, optical switches, fire alarm sensors and photovoltaic, photonic and optoelectronic cells are known and have been repeatedly described.[171, 172, 180–187] The application of nanostructured lead sulfide is exemplified in Fig. 26, which shows a photograph of a flexible photodetector based on paper covered by a layer of PbS quantum dots.[184] Nanostructured PbS has been used as the key working part in systems of detection of extraterrestrial objects by their thermal emission and in the operated and autonomous (unaided) target guidance systems.

Less widely known is the use of nanostructured PbS as a solid-phase sensor for detection of gases [CO, CO_2, SO_2, N_2, NO and especially NO_2 and NH_3 (see Refs 188–192)], for monitoring of heavy metals, including lead, in aqueous media.[193, 194] Polymeric matrices with PbS nanoparticles are used for protection from γ-radiation.[195, 196]

As a result of active integration of the achievements of chemistry, biology and medicine, a background for biomedical applications and development of more perfect tools for medical diagnosis and therapy [197] using nanostructured lead sulfide has been created in the last decade. An example is provided by hybrid PbS nanoparticles coated by L-cysteine as a capping agent.[60] Of interest is the drug delivery to injured organs and tumour cells, which is a prerequisite for more successful therapy. For this purpose, it is especially promising to use core–shell sulfide heteronanostructures.[198]

Enhancement of the luminescence intensity of the hybrid sulfide heteronanostructures based on PbS is attained owing to combination of luminescent sulfide nanoparticles with metal (especially silver) nanoparticles possessing the surface plasmon resonance. The injured areas can be visualized by using luminescent PbS quantum dots combined into a single nanostructure with organic drugs. Hybrid nanomaterials of this type based on PbS find use and are often indispensable in biosensorics, medicine, green chemistry and other areas.[198–201] Furthermore, the design of hybrid nanomaterials involving lead sulfide promotes elaboration of new analytical methods for the detection and identification of

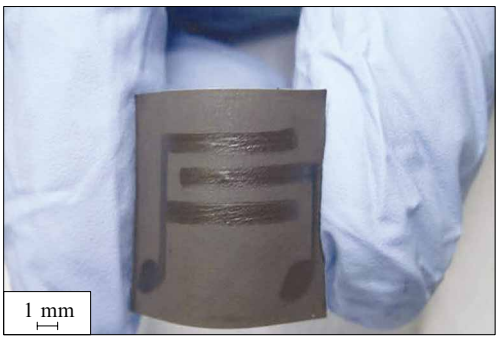


Figure 26. Photograph of flexible photodetector made of PbS quantum dots on a paper substrate.[184]

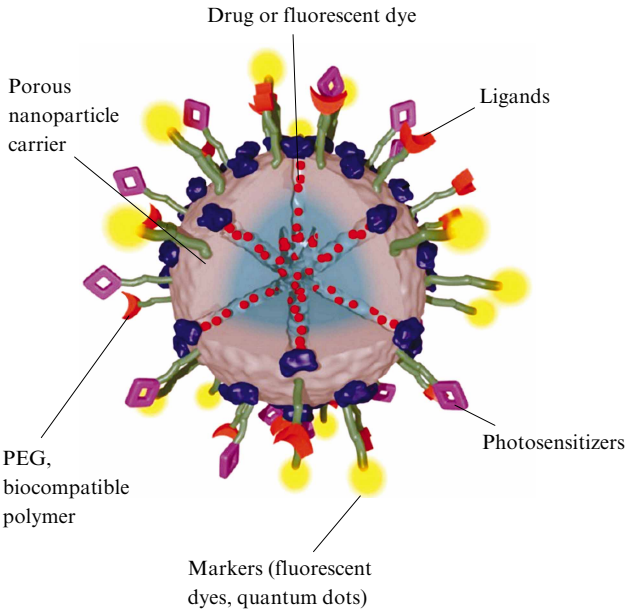


Figure 27. Schematic structure of a multifunctional hybrid nanostructure for biomedical applications based on a porous nanoparticle (*e.g.*, quartz) as a carrier.[204]

impurities, preconcentration and separation of compounds and visualization of biological action.[202–204] For example, in recent years, many reports have appeared about the successful synthesis and *in vivo* application of multifuctional hybrid nanostructures for the targeted drug delivery to damaged cells. Apart from other compounds, lead, cadmium and zinc sulfides are used in these structures as luminescent markers.

The multifunctional hybrid nanostructure proposed by Argyo *et al.*,[204] suitable for solving a whole range of biomedical problems is shown in Fig. 27. These multifunctional hybrid nanocomposite structures can be designed on the basis of nanostructures with highly developed surface, for example, mesoporous quartz and ceramic nanoparticles, graphene and carbon nanotubes, which form the central core. To the core surface, one can attach various drug molecules, fluorescent dyes or quantum dots functioning as markers. Numerous studies demonstrated that the core size preferred for drug or marker delivery is less than 120 nm. Coating of the central core by various organic shells increases the biocompatibility of multifunctional hybrid nanostructures because of the fact that the organic polymer shell contains active groups for the attachment of biological molecules (antibodies, peptides, DNA and so on).

Lead sulfide nanoparticles embedded in multi-walled carbon nanotubes have been proposed as highly sensitive genomic sensors for the detection of pathogenic bacteria.[205]

In parallel with the studies devoted to biomedical applications of PbS nanoparticles, the toxicity of nanostructured lead sulfide was studied;[206, 207] the results confirmed the applicability of these particles in living organisms provided that the PbS particles are coated by protective biologically harmless shells.

The key principles and approaches developed for the synthesis and investigations of various forms of nanostructured lead sulfide are used in relation to other nanocrystal-

line compounds ranging from sulfides to oxides and carbides. For example, the effect of the small particle size on the thermal expansion and non-stoichiometry of nanocrystalline Ag_2S has been considered in a number of publications [208 – 210] using an approach proposed previously [162, 163] for nanostructured PbS. Modification of optical and electronic properties of indium and gallium oxide nanofilms has been considered by Chen *et al.*,[211] who took into account data of a study of PbS films.[98] The relationship between the non-stoichiometry, ordering and small particle size in the cubic titanium monoxide obtained in the nanocrystalline state by high-energy milling has been discussed.[212 – 214] Details of the structure and preparation of nanocrystalline non-stoichiometric carbides, taking account of their homogeneity, as well as of oxide nanoceramics have been reported.[215 – 222]

VI. Conclusion

The advances in science and technology of the first half of the 21st century will be stipulated by the development of electronics and computational, bio- and nanotechnologies. The research into the nanomaterials and nanotechnologies related to semiconducting chalcogenides, including sulfides, has been developed especially actively in the last two decades. The main effort has been directed towards the development of methods for the synthesis of nanostructured sulfides with controlled geometric and morphological characteristics.

The interest in the nanostructured lead sulfide that arouse at the end of the 20th century is due to the potential application of PbS in optoelectronics, power engineering, manufacture of solid-phase sensors for various gases, design of polymer composite materials with enhanced radiation stability owing to the addition of PbS nanoparticles and in biosensorics.

The data presented in the review indicate that nanostructured lead sulfide offers broad opportunities for the control of electronic, optical and thermal properties owing to size effects and large interfacial areas. The relatively large exciton radius (18 – 23 nm) in lead sulfide ensures quantum confinement in rather large quantum dots and intense emission in the near IR-range. Owing to their lower toxicity compared with the quantum dots based on cadmium, mercury, tellurium and selenium compounds, the stable water-soluble PbS quantum dots are considered as possible biolabels to study living organisms.

Nanostructured PbS acquire desirable properties when synthesized by processes that ensure the controlled size of structure elements and passivation of the surface. Among numerous methods of synthesis of nanostructured PbS, these conditions are met by deposition from aqueous solutions, which is implemented in many ways. Synthesis in water makes it possible to avoid the influence of toxic organic ligands or toxic organic solvents on biological objects when PbS quantum dots are utilized as biolabels. It can be expected that further development of the methods for the synthesis of PbS nanoparticles of specified size and shape would extend the scope of their applicability, in particular, in optoelectronics, biology and medicine.

This review was written with financial support of the Russian Foundation for Basic Research (Grant No. 13-08-00184a).

References

1. A Zakery, S R Elliott *J. Non-Cryst. Solids* **330** 1 (2003)
2. H Fu, S-W Tsang *Nanoscale* **4** 2187 (2012)
3. M-R Gao, Y-F Xu, J Jiang, S-H Yu *Chem. Soc. Rev.* **42** 2986 (2013)
4. *Nanomaterials: Synthesis, Properties and Applications* (Eds A S Edelstein, R C Cammarata) (London: Institute of Physics, 1996)
5. A I Gusev *Physics – Uspekhi* **41** 49 (1998) [*Usp. Fiz. Nauk* **168** 55 (1998)]
6. H Gleiter *Acta Mater.* **48** 1 (2000)
7. *Slovar' Nanotekhnologicheskikh i Svyazannykh s Nanotekhnologiyami Terminov* (Glossary of Nanotechnology and Nanotechnology-Related Terms) (Ed. S V Kalyuzhnyi) (Moscow: Fizmatlit, 2010)
8. A I Gusev, A A Rempel' *Nanokristallicheskie Materialy* (Nanocrystalline Materials) (Moscow: Fizmatlit, 2000)
9. A I Gusev, A A Rempel *Nanocrystalline Materials* (Cambridge: Cambridge International Science Publishing, 2004)
10. A I Gusev *Nanomaterialy, Nanostruktury, Nanotekhnologii* (Nanomaterials, Nanostructures, Nanotechnologies) (Moscow: Fizmatlit, 2009)
11. A A Rempel *Rus. Chem. Rev.* **76** 435 (2007)
12. H-E Schaefer *Nanoscience. The Science of the Small in Physics, Engineering, Chemistry, Biology and Medicine* (Heidelberg, Dordrecht, New York: Springer, 2010)
13. R F Khairutdinov *Russ. Chem. Rev.* **67** 109 (1998)
14. Zh I Alferov *Rev. Mod. Phys.* **73** 767 (2001)
15. A P Alivisatos *Science* **271** 933 (1996)
16. N N Ledentsov, V M Ustinov, V A Shchukin, P S Kop'ev, Zh I Alferov, D Bimberg *Semiconductors* **32** 343 (1998) [*Fiz. Tekh. Poluprovod.* **32** 385 (1998)]
17. T Theivasanthi, M Alagar *Res. Appl. Mater.* **1** 36 (2013)
18. A M Smith, S Nie *Acc. Chem. Res.* **43** 190 (2010)
19. G Hodes *Chemical Solution Deposition of Semiconductor Films* (New York: Marcel Dekker, 2002)
20. S M Pawar, B S Pawar, J H Kim, O-S Joo, C D Lokhande *Curr. Appl. Phys.* **11** 117 (2011)
21. D Deng, J Xia, J Cao, L Qu, J Tian, Z Qian *J. Colloid Interface Sci.* **367** 234 (2012)
22. B Zhang, G Li, J Zhang, Y Zhang, L Zhang *Nanotechnology* **14** 443 (2003)
23. I Chakraborty, S P Moulik *J. Nanopart. Res.* **7** 237 (2005)
24. Y Jiao *Mater. Lett.* **72** 116 (2011)
25. M R Karim, M D A Zaman, M D B Zaman *Chalcogen. Lett.* **11** 531 (2014)
26. F Li, X Huang, T Kong, X Liu, Q Qin, Z Li *J. Alloys Compd.* **485** 554 (2009)
27. G A Kitaev, T P Bol'shchikova, G M Fofanov, L E Yatlova, N M Goryukhina, in *Kinetika i Mekhanizm Obrazovaniya Tverdoi Fazy* (Kinetics and Formation Mechanism of the Solid Phase) (Sverdlovsk: Ural Pedagogical Institute, 1968) p. 113
28. A P Gaiduk, P I Gaiduk, A N Larsen *Thin Solid Films* **516** 3791 (2008)
29. J Wang, S H Tang, B Y Wang, Y Q Li *Sci. China Chem.* **56** 1593 (2013)
30. S I Sadovnikov, Yu V Kuznetsova, A A Rempel *Inorg. Mater.* **50** 969 (2014) [*Neorg. Mater.* **50** 1049 (2014)]
31. S I Sadovnikov, A I Gusev *J. Alloys Compd.* **586** 105 (2014)
32. N S Kozhevnikova, S I Sadovnikov, A A Rempel *Russ. J. Gen. Chem.* **81** 2062 (2011) [*Zh. Obshch. Khim.* **81** 1608 (2011)]
33. Patent RF 2567326 (2015)
34. M Froment, D Lincot *Electrochem. Acta* **40** 1293 (1995)

35. R A Yusupov, R F Abzalov, S G Smerdova, M R Gafarov *Chem. Comput. Simul. Butlerov Commun.* **1** (3) 29 (2000) [*Khim. Komp. Modelirovanie. Butlerovskie Soobshcheniya* (3) **1** 29 (2000)]
36. P O'Brien, T Saeed *J. Cryst. Growth* **158** 497 (1996)
37. P O'Brien, J McAleese *J. Mater. Chem.* **8** 2309 (1998)
38. A Osherov, V Ezersky, Y Golan *J. Cryst. Growth* **308** 334 (2007)
39. P M A de Farias, D Saegesser Santos, F D de Menezes, R de Carvalho Ferreira, M de Lourdes Barjas-Castro, V Castro, P R Moura Lima, A Fonte, C L Cesar *J. Microscop.* **219** 103 (2005)
40. N S Kozhevnikova, S I Sadovnikov, A A Uritskaya, A I Gusev *Izv. Vyssh. Uchebn. Zaved., Khim. Kkhim. Tekhnol.* **55** (3) 13 (2012)
41. N S Kozhevnikova, S I Sadovnikov, A A Uritskaya, A I Gusev *Rus. J. Gen. Chem.* **82** 626 (2012) [*Zh. Obshch. Khim.* **82** 538 (2012)]
42. K J Powell, P L Brown, R H Byrne, T Gajda, G Hefter, A-K Leuz, S Sjoberg, H Wanner *Pure Appl. Chem.* **81** 2425 (2009)
43. V F Markov, L N Maskaeva, P N Ivanov *Kondensirovannye Sredy i Mezhfaznye Granitsy* **6** 374 (2004)
44. Y Wang Y , L Chai, H Chang, X Peng, Y Shu *Trans. Nonferrous Met. Soc. China* **19** 458 (2009)
45. V N Semenov, N M Ovechkina, D A Khoviv *Vestn. Voronezh. Gos. Univ., Ser. Khim., Biol., Farmatsiya* (2) 50 (2007)
46. L D Pettit, K J Powell *The IUPAC Stability Constants Database (SC-Database Release 5.8 for Windows)* (Ottley, UK: Academic Software and K J Powell, 2009) www.acadsoft.co.uk
47. S I Sadovnikov, A I Gusev *Russ. J. Gen. Chem.* **84** 173 (2014) [*Zh. Obshch. Khim.* **84** 177 (2014)]
48. S I Sadovnikov, A I Gusev *Inorg. Mater.* **51** 1219 (2015) [*Neorg. Mater.* **51** 1313 (2015)]
49. Yu Yu Lur'e, in *Spravochnik po Analiticheskoi Khimii* (Handbook on Analytical Chemistry) (Moscow: Khimiya, 1967) p. 101
50. P Patnaik *Dean's Analytical Chemistry Handbook* (New York: McGraw-Hill, 2004) Table 4.2.
51. Y Noda, S Ohba, S Sato, Y Saito *Acta Crystallogr., Sect. B* **39** 312 (1983)
52. Y Noda, K Masumoto, S Ohba, Y Saito, K Toriumi, Y Iwata, K Shibuya *Acta Crystallogr., Sect. C* **43** 1443 (1987)
53. A A Rempel, N S Kozhevnikova, A J G Leenaers, S van den Berghe *J. Cryst. Growth* **280** 300 (2005)
54. Y Jiang, Y Wu, B Xie, S W Yuan, X M Liu *J. Cryst. Growth* **231** 248 (2001)
55. Y J Yang, L Y He, Q F Zhang *Electrochem. Commun.* **7** 361 (2005)
56. M Sharon, K S Ramaiaha, M Kumar, M Neumann-Spallart, C Levy-Clement *J. Electroanal. Chem.* **436** 49 (1997)
57. Y J Yang *Mater. Sci. Eng., B* **131** 200 (2006)
58. N Pellegri, R Trbojevich, O de Sanctis *J. Sol-Gel Sci. Technol.* **8** 1023 (1997)
59. L Xu, X Chen, L Wang, Z M Sui, J Zhao, B Zhu *Colloids Surf., A* **257 – 258** 457 (2005)
60. Y Yu, K Zhang, S Sun *Appl. Surf. Sci.* **258** 7181 (2012)
61. D Gerion, F Pinaud, S C Williams,W J Parak, D Zanchet, S Weiss, A P Alivisatos *J. Phys. Chem. B* **105** 8861 (2001)
62. X Gao, Y Cui, R M Levenson, L W K Chung, S Nie *Nat. Biotechnol.* **22** 969 (2004)
63. R Sathyamoorthy, L Kungumadevi *Adv. Powder Technol.* **26** 355 (2015)
64. B Ding, M Shi, F Chen, R Zhou, M Deng, M Wang, H Z Chen *J. Cryst. Growth* **311** 1533 (2009)
65. H Emadi, M Salavati-Niasari *Superlatt. Microstruct.* **54** 118 (2013)
66. Y Ni, H Liu, F Wang, Y Liang, J Hong, X Ma, Z Xu *Cryst. Growth Des.* **4** 759 (2004)
67. Q Huang, L Gao *Chem. Lett.* **33** 1338 (2004)
68. P T Zhao, G Chen, Y Hu, X L He, K Wu, Y Cheng, K X Huang *J. Cryst. Growth* **303** 632 (2007)
69. Y Ma, L Qi, J Ma, H Cheng *Cryst. Growth Des.* **4** 351 (2004)
70. Y H Ding, X X Liu, R Guo *Colloids Surf., Sect. A* **296** 8 (2007)
71. E Leontidis, M Orphanou, T Kyprianidou-Leondidou, F Krumeich, W Caseri *Nano Lett.* **3** 569 (2003)
72. C Li, G Shi, H Xu, Sh Guang, R Yin, Y Song *Mater. Lett.* **61** 1809 (2007)
73. W Wang, Q Li, M Li, H Lin, L Hong *J. Cryst. Growth* **299** 17 (2007)
74. J-Q Sun, X-P Shen, L-J Guo, K-M Chen, Q Liu *Physica E* **41** 1527 (2009)
75. J Jiao, X Liu, W Gao, C Wang, H Feng, X Zhao, L Chen *Solid State Sci.* **11** 976 (2009)
76. M Shakouri-Arani, M Salavati-Niasari *J. Ind. Eng. Chem.* **20** 3141 (2014)
77. M Wu, H Zhong, Z Jiao, Z Li, Y Sun *Colloids Surf., Sect. A* **313 – 314** 35 (2008)
78. M Mozafari, F Moztarzadeh, A M Seifalian, L Tayebi *J. Lumin.* **133** 188 (2013)
79. A Schiener, T Wlochowitz, S Gerth, T Unruh, A Rempel, H Amenitsch, A Magerl *MRS Proc.* **1528** 1 (2013)
80. A Schiener, A Magerl, A Krach, S Seifert, H-G Steinrmck, J Zagorac, D Zahn, R Weihrich *Nanoscale* **7** 11328 (2015)
81. T Okuno, A A Lipovskii, T Ogawa, I Amagai, Y Masumoto *J. Lumin.* **87 – 89** 491 (2000)
82. K Wundke, J Auxier, A Schüulzgen, N Peyghambarian, N F Borrelli *Appl. Phys. Lett.* **75** 3060 (1999)
83. A M Malyarevich, M S Gaponenko, V G Savitski, K V Yumashev, G E Rachkovskaya, G B Zakharevich *J. Non-Cryst. Solids* **353** 1195 (2007)
84. X Kai, H Jong *J. Non-Cryst. Solids* **387** 76 (2014)
85. F del Monte, Y Xu, J D Mackenzie *J. Sol–Gel Sci. Technol.* **17** 37 (2000)
86. M Pinero, N de la Rosa-Fox, R Erge-Montilla, L Esquivias *J. Sol–Gel Sci. Technol.* **26** 527 (2003)
87. T D Krauss, F W Wise, D B Tanner *Phys. Rev. Lett.* **76** 1376 (1996)
88. A Haché, S-É LeBlanc, M LoCascio, A Martucci *Physica E* **17** 104 (2003)
89. B Ullrich, J S Wang *J. Lumin.* **143** 645 (2013)
90. Y Yu, K Zhang, S Sun *J. Mol. Struct.* **1031** 194 (2013)
91. E Pentia, L Pintilie, I Matei, T Botila, I Pintilie *Infrared Phys. Technol.* **44** 207 (2003)
92. G Hodes *Phys. Chem. Chem. Phys.* **9** 2181 (2007)
93. S I Sadovnikov, A I Gusev, A A Rempel *J. Exp. Theor. Phys. Lett.* **89** 238 (2009) [*Pis'ma Zh. Eksp. Teor. Fiz.* **89** 279 (2009)]
94. S I Sadovnikov, A A Rempel *Phys. Solid State* **51** 2375 (2009) [*Fiz. Tv. Tela* **51** 2237 (2009)]
95. S I Sadovnikov, N S Kozhevnikova, A I Gusev *Semiconductors* **45** 1559 (2011) [*Fiz. Tekh. Poluprovod.* **45** 1621 (2011)]
96. S I Sadovnikov, N S Kozhevnikova, V G Pushin, A A Rempel *Inorg. Mater.* **48** 21 (2012) [*Neorg. Mater.* **48** 26 (2012)]
97. S I Sadovnikov, N S Kozhevnikova *Phys. Solid State* **54** 1554 (2012) [*Fiz. Tv. Tela* **54** 1459 (2012)]
98. S I Sadovnikov, A I Gusev *J. Alloys Compd.* **573** 65 (2013)
99. Patent RF 2553858 (2015)
100. N I Fainer, M L Kosinova, Yu M Rumyantsev, E G Salman, F A Kuznetsov *Thin Solid Films* **280** 16 (1996)
101. R R Chamberlin, J S Sharman *J. Electrochem. Soc.* **113** 86 (1966)
102. B Thangaraju, P Kaliannan *Cryst. Res. Technol.* **35** 71 (2000)

103. Y F Nicolau *Appl. Surface Sci.* **22** – **23** 1061 (1985)
104. Patent US 4675207 (1987)
105. T Kanniainen, S Lindroos, J Ihanus, M Leskelä *J. Mater. Chem.* **6** 161 (1996)
106. J Puišo, S Tamulevičius, G Laukaitis, S Lindroos, M Leskelä, V Snitka *Thin Solid Films* **403** – **404** 457 (2002)
107. J Puičo, S Lindroos, S Tamulevičius, M Leskelä, V Snitka *Thin Solid Films* **428** 223 (2003)
108. K C Preetha, K V Murali, A J Ragina, K Deepa, T L Remadevi *Curr. Appl. Phys.* **12** 53 (2012)
109. E Yucel, Y Yucel, B Beleli *J. Cryst. Growth* **422** 1 (2015)
110. P K Nair, V M Garcia, A B Hernandez, M T S Nair *J. Phys. D* **24** 1466 (1991)
111. M A Zhukovskiy, A L Stroyuk, V V Shvalagin, N P Smirnova, O S Lytvyn, A M Eremenko *J. Photochem. Photobiol. A* **203** 137 (2009)
112. V P Ananikov, L L Khemchyan, Y V Ivanova, V I Bukhtiyarov, A M Sorokin, I P Prosvirin, S Z Vatsadze, A V Medved'ko, V N Nuriev, A D Dilman, V V Levin, I V Koptyug, K V Kovtunov, V V Zhivonitko, V A Likholobov, A V Romanenko, P A Simonov, V G Nenajdenko, O I Shmatova, V M Muzalevskiy, M S Nechaev, A F Asachenko, O S Morozov, P B Dzhevakov, S N Osipov, D V Vorobyeva, M A Topchiy, M A Zotova, S A Ponomarenko, O V Borshchev, Y N Luponosov, A A Rempel, A A Valeeva, A Y Stakheev, O V Turova, I S Mashkovsky, S V Sysolyatin, V V Malykhin, G A Bukhtiyarova, A O Terent'ev, I B Krylov *Russ. Chem. Rev.* **83** 885 (2014)
113. J-H Chen, C-G Chao, J-C Ou, T-F Liu *Surface Sci.* **601** 5142 (2007)
114. J C Lin, R C Sharma, Y A Chang *Bull. Alloys Phase Diagr.* **7** 374 (1986)
115. S B Qadri, J Yang, B R Ranta, E F Skelton *Appl. Phys. Lett.* **69** 2205 (1996)
116. K Knorr, L Ehm, M Hytha, B Winkler, W Depmeier *Eur. Phys. J., B* **31** 297 (2003)
117. J Zhang, L Sun, S Liao, C Yan *Solid State Commun.* **124** 45 (2002)
118. H Metin, R Esen *J. Cryst. Growth* **258** 141 (2003)
119. G S Wu, X Y Yuan, T Xie, G C Xu, L D Zhang, Y L Zhuang *Mater. Lett.* **58** 794 (2004)
120. A S Vorokh, A A Rempel *Phys. Solid State* **49** 148 (2007) [*Fiz. Tv. Tela* **49** 143 (2007)]
121. A A Rempel, A Magerl *Acta Crystallogr., Sect. A* **66** 479 (2010)
122. S B Qadri, A Singh, M Yousuf *Thin Solid Films* **431** – **432** 506 (2003)
123. F A Fernandez-Lima, Y Gonzalez-Alfaro, E M Larramendi, H D Fonseca Filho, M E H Maia da Costa, F L Freire Jr, R Prioli, R R de Avillez, E F da Silveira, O Calzadilla, O de Melo, E Pedrero, E Hernández *Mater. Sci. Eng., B* **136** 187 (2007)
124. Y Gotoh, M Onoda, M Goto, Y Oosawa *Chem. Lett.* **18** 1281 (1989)
125. G A Wiegers, A Meetsma, R J Haange, S van Smaalen, J L de Boer, A Meerschaut, P Rabu, J Rouxel *Acta Crystallogr., Sect. B* **46** 324 (1990)
126. J Wullf, A Meetsma, S van Smaalen, R J Haange, J L de Boer, G A Wiegers *J. Solid State Chem.* **84** 118 (1990)
127. G A Wiegers *Prog. Solid State Chem.* **24** 1 (1996)
128. S I Sadovnikov, A A Rempel *Dokl. Phys. Chem.* **428** 167 (2009) [*Dokl. Akad. Nauk* **428** 48 (2009)]
129. H M Rietveld *J. Appl. Cryst.* **2** 65 (1969)
130. S I Sadovnikov, A A Rempel *Phys. Solid State* **52** 2458 (2010) [*Fiz. Tv. Tela* **52** 2299 (2010)]
131. T S Moss *Optical Properties of Semiconductors* (Ed. C A Hogarth) (London: Butterworths Sci. Publ., 1959)
132. R B Schoolar, J R Dixon *Phys. Rev.* **137** 667 (1965)
133. J N Zemmel, J D Jensen, R B Schoolar *Phys. Rev.* **140** 330 (1965)
134. Yu I Ukhanov *Opticheskie Svoistva Poluprovodnikov* (Optical Properties of Semiconductors) (Moscow: Nauka, 1977)
135. A I Gusev *Nanokristallicheskie Materialy: Metody Polucheniya i Svoistva* (Nanocrystalline Materials: Methods of Synthesis and Properties) (Ekaterinburg: Ural Branch of the Russian Academy of Sciences, 1998)
136. A Sashchiuk, E Lifshitz, R Reisfeld, T Saraidarov, M Zelner, A J Willenz *Sol – Gel Sci. Technol.* **24** 31 (2002)
137. B Yu, G Yin, C Zhu, F Gan *Opt. Mater.* **11** 17 (1998)
138. S Jana, R Thapa, R Maity, K K Chattopadhyay *Physica E* **40** 3121 (2008)
139. L E Brus *J. Chem. Phys.* **80** 4403 (1984)
140. Y Wang, N Herron *J. Chem.* **95** 525 (1991)
141. M Najdovski, B Minceva-Sukarova, A Drake, I Grozdanov, C J Chunnilall *J. Mol. Struct.* **349** 85 (1995)
142. R S Parra, P J George, G G Svnchez, A E Jiménez González, L Baños, P K Nair *J. Phys. Chem. Solids* **61** 659 (2000)
143. J J Valenzuel-Jaureguia, R Ramírez-Bon, A Mendoza-Galvan, M Sotelo-Lerma *Thin Solid Films* **441** 104 (2003)
144. J J Peterson, T D Krauss *Nano Lett.* **6** 510 (2006)
145. Y Zhao, J Zou, W Shi *Mater. Sci. Eng., B* **121** 20 (2005)
146. S I Sadovnikov, N S Kozhevnikova, A A Rempel *Semiconductors* **44** 1349 (2010) [*Fiz. Tekh. Poluprovod.* **44** 1394 (2010)]
147. *Amorphous and Liquid Semiconductors* (Ed. J Tauc) (New York: Plenum, 1974)
148. C F Klingshirn *Semiconductor Optics* (New York: Springer, 2005)
149. A S Kurlov, A I Gusev *Phys. Rev. B* **76** Art. No 174115 (2007)
150. R J Elliot *Phys. Rev.* **108** 1384 (1957)
151. D M Mittleman, R W Schoenlein, J J Shiang, V L Colvin, A P Alivisatos, C V Shank *Phys. Rev. B* **49** 14435 (1994)
152. D Kumar, G Agarwal, B Tripathi, D Vyas, V Kulshrestha *J. Alloys Compd.* **484** 463 (2009)
153. In *Landolt-Börnstein: Zahlenwerte und Funktionen aus Naturwissenschaften und Technik. Neue Serie. Grouppe III: Kristall- und Festkorperphysik* Bd. 17f (Eds K-H Hellwege, O Madelung) (Berlin, Heidelberg, New York, Tokyo: Springer, 1983) p. 155
154. Z Q Mamiyev, N O Balayeva *Opt. Mater.* **46** 522 (2015)
155. Y Wang, A Suna, W Mahier, R Kasowski *J. Chem. Phys.* **87** 7315 (1987)
156. E Lifshitz, M Sirota, H Porteanu *J. Cryst. Growth* **196** 126 (1999)
157. M Navaneethan, M Sabarinathan, S Harish, J Archana, K D Nisha, Y Hayakawa, S Ponnusamy, C Muthamizhchelvan *Mater. Lett.* **158** 75 (2015)
158. S S Sharma *Proc. Indian Acad. Sci., Sect. A* **34** 72 (1951)
159. S I Novikova, N Kh Abrikosov *Fiz. Tv. Tela* **5** 1913 (1963)
160. Y Zhang, X Ke, C Chen, J Yang, P R C Kent *Phys. Rev. B* **80** 024304 (2009)
161. S I Sadovnikov, N S Kozhevnikova, A A Rempel, A Magerl *Thin Solid Films* **548** 230 (2013)
162. S I Sadovnikov, A I Gusev *J. Alloys Compd.* **610** 196 (2014)
163. S I Sadovnikov, A I Gusev *Phys. Solid State* **56** 2353 (2014) [*Fiz. Tv. Tela* **56** 2274 (2014)]
164. Yu I Petrov *Fizika Malykh Chastits* (The Physics of Small Particles) (Moscow: Nauka, 1982)
165. E W Montroll *J. Chem. Phys.* **18** 183 (1950)
166. A A Chudinov *Fiz. Tv. Tela* **5** 1458 (1963)
167. V Padaki, S Lakshimikumar, S Subramanyam, E Gopal *Pramana J. Phys.* **17** 25 (1981)
168. W Li, J-F Chen, T Wang *Physica B* **405** 1279 (2010)
169. P Bhardwaj *ISRN Cond. Matter Phys.* **2012** 596397 (2012)
170. N Choudhury, B K Sarma *Bull. Mater. Sci.* **32** 43 (2009)

171. E I Grigor'ev, S A Zav'yalov, S N Chvalun *Ros. Nanotekhnol.* (1) 58 (2006)
172. A Levchenko, L Leonova, Yu Dobrovol'skii *Elektronika: Nauka Tekhnologiya Biznes* (1) 66 (2008)
173. S I Sadovnikov, N S Kozhevnikova, A A Rempel *Glass Phys. Chem.* **35** 60 (2009) [*Fiz. Khim. Stekla* **35** 74 (2009)]
174. S I Sadovnikov, N S Kozhevnikova, A A Rempel *Russ. J. Inorg. Chem.* **56** 1864 (2011) [*Zh. Neorg. Khim.* **56** 1951 (2011)]
175. S I Sadovnikov, N S Kozhevnikova, A A Rempel *Inorg. Mater.* **47** 837 (2011) [*Neorg. Mater.* **47** 929 (2011)]
176. V Y Gertsman, R Birringer, R Z Valiev, H Gleiter. *Scr. Metall Mater.* **30** 229 (1994)
177. G S Frents *Okislenie Sul'fidov Metallov* (Oxidation of Metal Sulfides) (Moscow: Nauka, 1964)
178. Yu L Mikhlin, A S Romanchenko, A A Shagaev *Appl. Surf. Sci.* **252** 5645 (2006)
179. R Ihly, J Tolentino, Y Liu, M Gibbs, M Law *ACS Nano* **5** 8175 (2011)
180. V M García, M T S Nair, P K Nair *Sol. Energy Mater.* **23** 47 (1991)
181. P K Nair, O Gomezdaza, M T S Nair *Adv. Mater. Opt. Electron.* **1** 139 (1992)
182. P A Loiko, G E Rachkovskaya, G B Zakharevich, V S Gurin, M S Gaponenko *J. Non-Cryst. Solids* **358** 1840 (2012)
183. A Carrillo-Castillo, A Salas-Villasenor, I Mejia, S Aguirre-Tostado, B E Gnade, M A Quevedo-Lopez *Thin Solid Films* **520** 3107 (2012)
184. J He, M Luo, L Hu, Y Zhou, S Jiang, H Song, R Ye, J Chen, L Gao, J Tang *J. Alloys Compd.* **596** 73 (2014)
185. A Slonopas, N Alijabbari, C Saltonstall, T Globus, P Norris *Electrochim. Acta* **151** 140 (2015)
186. M Sabet, M Salavati-Niasari *Electrocim. Acta* **169** 168 (2015)
187. J Jang, J H Song, Y Choi, S J Baik, S Jeong *Sol. Energy Mater. Sol. Cells* **141** 270 (2015)
188. V F Markov, L N Maskaeva *J. Anal. Chem.* **56** 754 (2001)
189. T Fu *Sens. Actuators, B* **140** 116 (2009)
190. S Bandyopadhyay *Part. Sci. Technol.* **30** 43 (2012)
191. H Karami, M Ghasemi, S Matini *Int. J. Electrochem. Sci.* **8** 11661 (2013)
192. S Kaci, A Keffous, S Hakoum, A Mansri *Vacuum* **116** 27 (2015)
193. T Kullick, R Quack, C Röhrkasten, T Pekeler, T Scheper, K Schügerl *Chem. Eng. Technol.* **18** 225 (1995)
194. V F Markov, L N Maskaeva , I V Zurabin, N V Zamaraeva *Voda: Khim. Ekol.* (6) 80 (2012)
195. Y Xie, Z Qiao, M Chen, Y Zhu Y Qian *Chem. Lett.* **9** 875 (1999)
196. O P Garcia, M C C de Albuquerque, K A da Silva Aquino, P L B de Araujo, E S de Araujo *Mater. Res.* **18** 365 (2015)
197. M P Kirpichnikov, S N Kochetkov *Russ. Chem. Rev.* **84** E01 (2015)
198. A V Povolotskaya, A V Povolotskii, A A Man'shina *Russ. Chem. Rev.* **84** 579 (2015)
199. X Wang, X Li, D Liu, Sh Song, H Zhang *Chem. Commun.* **48** 2885 (2012)
200. S Narayanan, B N Sathy, U Mony, M Koyakutty, S V Nair, D Menon *ACS Appl. Mater. Interfaces* **4** 251 (2012)
201. H Genuino, H Huang, E Njagi, L Stafford, S L Suib, in *Handbook of Green Chemistry* Vol. 8 (Eds A Perosa, M Selva) (Weinheim: Wiley-VCH, 2012) p. 217
202. A Shen, L Chen, W Xie, J Hu, A Zeng, R Richards, J Hu *Adv. Funct. Mater.* **20** 969 (2010)
203. Y J Lu, K C Wei, C C Ma, S Y Yang, J P Chen *Colloids Surf., B* **89** 1 (2012)
204. C Argyo, V Weiss, C Braeuchle, T Bein *Chem. Mater.* **26** 435 (2014)
205. A M Fernandes, M H Abdalhai, J Ji, B-W Xi, J Xie, J Sun, R Noeline, B H Lee, X Sun *Biosens. Bioelectron.* **63** 399 (2015)
206. Q Li, X Hu, Y Bai, M Alattar, D Ma, Y Cao, Y Hao, L Wang, C Jiang *Food Chem. Toxicol.* **60** 213 (2013)
207. Y Cao, H Liu, Q Li, Q Wang, W Zhang, Y Chen, D Wang, Y Cai *J. Inorg. Biochem.* **126** 70 (2013)
208. S I Sadovnikov, A I Gusev, A A Rempel *Phys. Chem. Chem. Phys.* **17** 12466 (2015)
209. A I Gusev, S I Sadovnikov, A V Chukin, A A Rempel *Phys. Solid State* **58** 251 (2016) [*Fiz. Tv. Tela* **58** 249 (2016)]
210. S I Sadovnikov, A I Gusev, A V Chukin, A A Rempel *Phys. Chem. Chem. Phys.* **18** 4617 (2016)
211. X F Chen, G He, M Liu, J W Zhang, B Deng, P H Wang, M Zhang, J G Lv, Z Q Sun *J. Alloys Compd.* **615** 636 (2014)
212. A A Valeeva, A A Rempel, A I Gusev *J. Exp. Thepr. Phys. Lett.* **71** 460 (2000) [*Pis'ma Zh. Eksp. Teor. Fiz.* **71** 675 (2000)]
213. A A Valeeva, A A Rempel, A Pfitzner *Monat. Chem.* **146** 1205 (2015)
214. A A Valeeva, R A Petrovykh, H Schroettner, A A Rempel *Inorg. Mater.* **51** 1132 (2015) [*Neorg. Mater.* **51** 1221 (2015)]
215. A I Gusev, A A Rempel, V N Lipatnikov *Phys. Status Solidi A.* **106** 459 (1988)
216. A A Rempel, A I Gusev *Phys. Solid State* **42** 1280 (2000) [*Fiz. Tv. Tela* **42** 1243 (2000)]
217. A S Kurlov, A I Gusev *Tech. Phys.* **56** 975 (2011) [*Zh. Tekh. Fiz.* **81** 76 (2011)]
218. K C Singh, A K Nath *Mater. Lett.* **65** 970 (2011)
219. A M Minaev, D M Mordasov, L N Tyalina *Tech. Phys.* **58** 1604 (2013) [*Zh. Tekh. Fiz.* **83** 56 (2013)]
220. A I Gusev, A S Kurlov, T D Bel'kova, A M Bel'kov *Int. J. Ref. Met. Hard Mater.* **51** 70 (2015)
221. A Vinesh, V D Sudheesh, V Sebastian, N Lakshmi, K Venugopalan *J. Magn. Magn. Mater.* **386** 129 (2015)
222. A S Kurlov, A I Gusev, E Yu Gerasimov, I A Bobrikov, A M Balagurov, A A Rempel *Superlatt. Microstr.* **90** 148 (2016)